JEM Journal of Experimental Medicine

BRIEF DEFINITIVE REPORT

SARS-CoV-2 Spike protein suppresses CTL-mediated killing by inhibiting immune synapse assembly

Anna Onnis[1], Emanuele Andreano[2], Chiara Cassioli[1], Francesca Finetti[1], Chiara Della Bella[3], Oskar Staufer[4], Elisa Pantano[2], Valentina Abbiento[2], Giuseppe Marotta[5], Mario Milco D'Elios[6], Rino Rappuoli[2,7], and Cosima T. Baldari[1]

CTL-mediated killing of virally infected or malignant cells is orchestrated at the immune synapse (IS). We hypothesized that SARS-CoV-2 may target lytic IS assembly to escape elimination. We show that human CD8⁺ T cells upregulate the expression of ACE2, the Spike receptor, during differentiation to CTLs. CTL preincubation with the Wuhan or Omicron Spike variants inhibits IS assembly and function, as shown by defective synaptic accumulation of TCRs and tyrosine phosphoproteins as well as defective centrosome and lytic granule polarization to the IS, resulting in impaired target cell killing and cytokine production. These defects were reversed by anti-Spike antibodies interfering with ACE2 binding and reproduced by ACE2 engagement by angiotensin II or anti-ACE2 antibodies, but not by the ACE2 product Ang (1-7). IS defects were also observed ex vivo in CTLs from COVID-19 patients. These results highlight a new strategy of immune evasion by SARS-CoV-2 based on the Spike-dependent, ACE2-mediated targeting of the lytic IS to prevent elimination of infected cells.

Introduction

Severe coronavirus disease 2019 (COVID-19) caused by SARS-CoV-2 infection is associated with immune dysregulation, with defective IFN type I response (Bastard et al., 2020; Zhang et al., 2020), local hyperactivation of innate immune cells, impaired adaptive immune responses, and a prominent role for T cells (Chen and John Wherry, 2020; Kalfaoglu et al., 2021). T cell defects include lymphopenia and dysfunctions that range from excessive activation and exhaustion to defective activation and abnormalities in differentiation (Chen and John Wherry, 2020; Kalfaoglu et al., 2021). Interestingly, CD8⁺ T cells appear preferentially dysregulated in severe COVID-19 compared with CD4⁺ T cells. A selective decrease in cytotoxic T lymphocytes (CTL) in the upper respiratory tract has been observed in patients with severe disease compared to patients with milder disease (Chua et al., 2020). Additionally, a decrease in cytokine production by CD8⁺ T cells has been reported in severe COVID-19 (Zheng et al., 2020), while a more robust CD8⁺ T cell expansion has been associated with milder disease or recovery (Liao et al., 2020; Wen et al., 2020).

As the T cell effectors responsible for the elimination of virally infected cells, CTLs are strategic targets for immune evasion by viral pathogens. Major components of the CTL killing arsenal are lytic granules (LG), lysosome-like organelles enriched in granzymes, and perforin that are secreted upon activation (Cassioli and Baldari, 2022). While specificity is dependent on cognate cell recognition by TCR interaction with MHCI-bound peptide antigen, selectivity is ensured by the precise delivery of the cytotoxic effectors to the target cell at the immune synapse (IS), a highly specialized signaling and secretory platform that forms at the CTL interface with its target (Douanne and Griffiths, 2021; Dustin and Choudhuri, 2016). TCR engagement triggers a profound rearrangement of receptors, adhesion molecules, and costimulatory receptors at the target cell contact, which leads to the typical bull's eye architecture of the mature IS. IS assembly is coordinated by the cytoskeleton. An inward actin flow allows for the centripetal movement of TCRs and costimulatory receptors to the IS center, eventually forming an F-actin ring that seals a space between the CTL and its target, the synaptic cleft. Additionally, the centrosome and secretory apparatus polarize toward the target cell, with microtubules providing tracks for the transport of the cytotoxic machinery to the IS for delivery into the synaptic cleft (Blumenthal and Burkhardt, 2020; Martin-Cofreces and Sanchez-Madrid, 2018).

Differentiation of CD8⁺ T cells to CTLs is primed in peripheral lymphoid tissues by DCs that have been activated at the site of

[1]Department of Life Sciences, University of Siena, Siena, Italy; [2]Monoclonal Antibody Discovery Lab, Fondazione Toscana Life Sciences, Siena, Italy; [3]Department of Experimental and Clinical Medicine, University of Florence, Florence, Italy; [4]Kennedy Institute of Rheumatology, Nuffield Department of Orthopaedics, Rheumatology and Musculoskeletal Science, University of Oxford, Oxford, UK; [5]Siena University Hospital, Siena, Italy; [6]Department of Molecular and Developmental Medicine, University of Siena, Siena, Italy; [7]Department of Biotechnology, Chemistry and Pharmacy, University of Siena, Siena, Italy.

Correspondence to Cosima T. Baldari: cosima.baldari@unisi.it; Rino Rappuoli: rino.rappuoli@biotecnopolo.it.

infection. Hence, the dysregulation of the CD8+ T response by SARS-CoV-2 is likely to result, at least in part, from defective priming. However, once differentiated, CTLs migrate to the site of infection, where they can be exposed to high virus concentrations. The finding that the SARS-CoV-2 receptor human angiotensin-converting enzyme 2 (ACE2; Hoffmann et al., 2020) is expressed in activated T cells and mediates SARS-CoV-2 binding and internalization (Welch et al., 2022) suggests that as a result of ACE2 engagement by the Spike protein, T cells may be directly modulated by the virus.

We have hypothesized that similar to viruses such as HIV-1 (Fackler et al., 2007), SARS-CoV-2 may target IS assembly and function as a means to escape CTL-mediated killing. We provide evidence that Spike suppresses IS assembly in CTLs, leading to impaired cytotoxicity and cytokine production. This effect is dependent on ACE2 interaction and can be reproduced by ACE2 ligands, identifying ligand-bound ACE2 as an inhibitory receptor in CTL activation and a target for immune evasion by SARS-CoV-2.

Results and discussion

CTLs express the Spike receptor ACE2

While activated T cells have been reported to express the Spike receptor ACE2 (Welch et al., 2022), whether this occurs in CTLs has not been investigated. We generated CTLs from CD8+ T cells immunopurified by negative selection from buffy coats from healthy donors and activated them using beads coated with anti-CD3 and anti-CD28 mAbs in the presence of IL-2 (Fig. S1 A). Under these conditions, CD8+ T cells differentiate to functional CTLs by day 5, as assessed by granzyme B (GzmB) expression and cytotoxicity (Fig. S1, B and C). Quantitative reverse transcription PCR (RT-qPCR) and immunoblot analyses showed that ACE2 was undetectable or barely detectable in freshly purified CD8+ T cells, but was strongly upregulated in CTLs (Fig. 1, A and B). Consistent with ACE2 expression, Spike was found to bind to CTLs but not freshly purified CD8+ T cells, as assessed by imaging CTLs incubated with Wuhan Spike (Spike W) and labeled with an anti-Spike mAb (Fig. 1 C). This was confirmed by imaging CTLs incubated with fluorescently labeled pseudoviral particles (minimal virions, MiniVs) assembled in vitro using small unilamellar vesicles with a lipid composition adjusted to resemble the virion lipid membrane and the Spike W ectodomain (~18–40 copies Spike/particle; Staufer et al., 2022; Fig. 1 D).

Spike suppresses IS formation and CTL-mediated cytotoxicity

To test the hypothesis that Spike binding to ACE2 modulates CTL function by targeting the IS, CTLs were pretreated for 30 min with different concentrations of Spike W at 20°C to allow for binding, but not internalization, and subsequently mixed with Raji B cells pulsed with a mix of the Staphylococcal enterotoxins A, B, and E to broadly cover the TCR Vβ repertoire. This is the experimental setting typically used to image IS assembly when using polyclonal human T cells. The experiment was carried out in the absence of serum to rule out the potential effects of circulating angiotensins (Ang).

The assembly of functional immune synapses was assessed by measuring the accumulation of tyrosine phosphoproteins and TCR/CD3 complexes at the T cell interface with the APC for 15 min following contact with target cells, a time point when the IS has acquired its characteristic architecture. Spike was found to suppress the formation of signaling-competent immune synapses by CTLs in a dose-dependent fashion, as shown by the decreased frequency of conjugates displaying PTyr staining at the IS and the impairment in the synaptic accumulation of tyrosine phosphoproteins (Fig. 1, E and F; Videos 1, 2, and 3; and Fig. S1, D and E). Spike also suppressed TCR/CD3 accumulation at the IS (Fig. 1, E and G; and Videos 1, 2, and 3), accounting for the downstream signaling defect. Similar results were obtained when CTLs were pretreated with MiniVs (Fig. 1, H and I).

TCR signaling starts immediately upon T cell contact with a cognate APC and is sustained throughout the process of IS maturation. To understand whether Spike interferes with TCR signaling at an earlier stage of IS maturation, we compared the outcome of CTL pretreatment with Spike W on IS assembly in 5-min (nascent IS) versus 15-min (mature IS) conjugates. The defects in phosphotyrosine signaling and TCR/CD3 accumulation at the IS were clearly detectable in 5-min conjugates (Fig. 2, A and B), indicating that Spike W impairs TCR signaling at an early step in IS formation. Consistent with this finding, the early synaptic accumulation of active ZAP-70, the protein tyrosine kinase responsible for coupling the TCR to the downstream tyrosine phosphorylation cascade (Au-Yeung et al., 2018), was compromised in Spike W–pretreated CTLs (Fig. 2 C). The phosphotyrosine signaling defects were confirmed by flow cytometric analysis (Fig. 2 D and Fig. S1 F). Of note, these defects were caused by the interference of Spike with TCR signaling and not by steric hindrance at the synaptic contact, as shown by the impairment in TCR-dependent Erk activation in Spike W–pretreated CTLs activated by TCR crosslinking in the absence of a target cell partner (Fig. 2 E).

Centrosome repositioning to the IS is essential for the polarized delivery of the cytotoxic effectors of CTLs to the target cell (Douanne and Griffiths, 2021). Costaining with anti-pericentrin (PCNT) and anti-GzmB antibodies (Abs) showed that centrosome polarization toward the IS was impaired in Spike W– or MiniV-pretreated CTLs, as assessed by measuring the distance of the centrosome from the IS center (Fig. 3, A–C; Videos 4, 5, and 6; and Fig. S1 D). Additionally, LG convergence toward the centrosome, which is required for efficient degranulation (Daniele et al., 2011; Mentlik et al., 2010), was impaired under these conditions (Fig. 3, A and D; Videos 4, 5, and 6; and Fig. S1 D).

The impact of Spike on CTL degranulation was initially tested by measuring the exposure at the plasma membrane of the LG marker LAMP1, which occurs following LG fusion with the plasma membrane. Spike W pretreatment did not affect the ability of CTLs to degranulate in the presence of SAg-pulsed Raji cells, as assessed on conjugates incubated with fluorescently labeled anti-LAMP1 mAb and analyzed by flow cytometry under nonpermeabilizing conditions (Fig. 3 E). The very low TCR activation threshold for Ca^{2+} mobilization (Irvine et al., 2002), which is essential for CTL degranulation, could account for the

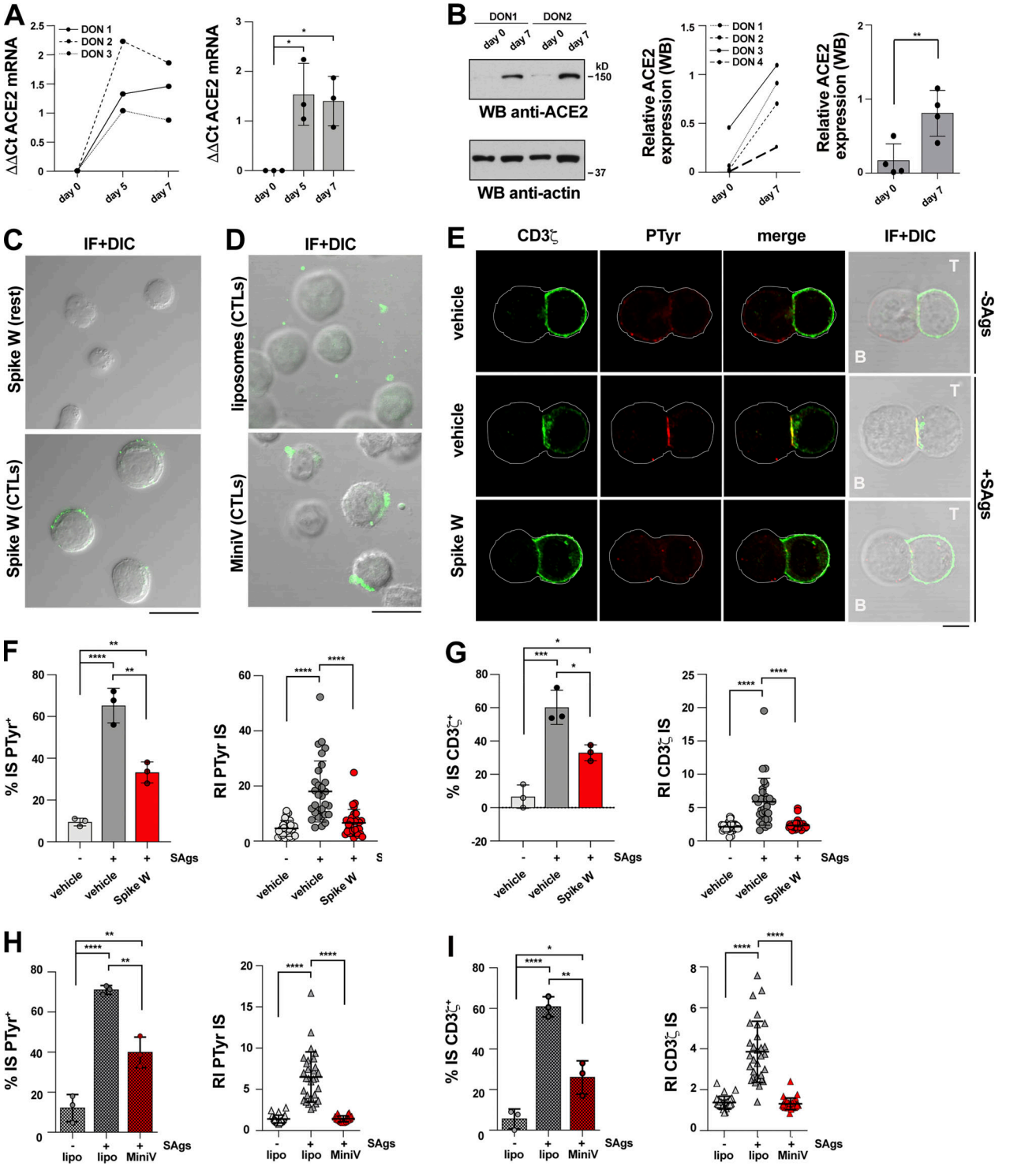

Figure 1. **Spike suppresses TCR accumulation and phosphotyrosine signaling at the CTL IS. (A and B)** RT-qPCR of human ACE2 mRNA (A) and immunoblot analysis of human ACE2 protein (B) in purified CD8⁺ T cells prior to stimulation (day 0) or after stimulation with anti-CD3/CD28 mAb–coated beads in the presence of IL-2 for the indicated times. The migration of molecular mass markers is indicated (n = 3, one-way ANOVA test for RT-qPCR analysis; *, P ≤ 0.05; n = 4, paired two-tailed Student's t test for immunoblot analysis; **, P ≤ 0.01). **(C)** Immunofluorescence analysis of Spike W binding to purified CD8⁺ T cells prior to stimulation (day 0) or 7 d after stimulation with anti-CD3/CD28 mAb–coated beads in the presence of IL-2 (n = 2). Scale bar, 15 µm. **(D)** Immunofluorescence analysis of CTL binding of fluorescently labeled MiniVs (Spike W embedded in fluorescent NDP-labeled liposomes) or control liposomes. Representative images are shown (n = 2). Scale bar, 15 µm. **(E–G)** Immunofluorescence analysis of CD3ζ and PTyr in CTLs (day 7) pretreated with either vehicle (PBS) or 0.05 µg/µl Spike W (cell viability after pretreatment 91.7 ± 0.2%), mixed with Raji cells (APCs) either unpulsed or pulsed with a combination of SEA, SEB, and SEE (SAgs), and incubated for 15 min at 37°C. Representative images (medial optical sections) of the T cell:APC conjugates are shown (E). Scale bar, 5 µm. **(F)** Left: Quantification (%) of 15-min SAg-specific conjugates harboring PTyr staining at the IS (≥50 cells/sample, n = 3, one-way ANOVA test; ****, P ≤ 0.0001; **, P ≤ 0.01). Right: Relative PTyr fluorescence intensity at the IS (recruitment index; 10 cells/sample, n = 3, Kruskal–Wallis test;

****, P ≤ 0.0001). **(G)** Left: Quantification (%) of 15-min SAg-specific conjugates harboring CD3ζ staining at the IS (≥50 cells/sample, *n* = 3, one-way ANOVA test; ***, P ≤ 0.001; *, P ≤ 0.05). Right: Relative CD3ζ fluorescence intensity at the IS (recruitment index; 10 cells/sample, *n* = 3, Kruskal–Wallis test; ****, P ≤ 0.0001). **(H and I)** Immunofluorescence analysis of CD3ζ and PTyr in CTLs (day 7) pretreated with either 1.2 × 10^9 control liposomes or MiniVs, mixed with Raji cells (APCs) either unpulsed or pulsed with a combination of SEA, SEB, and SEE (SAgs), and incubated for 15 min at 37°C. **(H)** Left: Quantification (%) of 15-min SAg-specific conjugates harboring PTyr staining at the IS (≥50 cells/sample, *n* = 3, one-way ANOVA test; ****, P ≤ 0.0001; **, P ≤ 0.01). Right: Relative PTyr fluorescence intensity at the IS (recruitment index; 10 cells/sample, *n* = 3, Kruskal–Wallis test; ****, P ≤ 0.0001). Side-by-side comparison of $PTyr^+$ immune synapses formed by CTLs pretreated with the same amount of soluble and MiniV-associated Spike showed a ∼2.3-fold increase in the suppressive ability of Spike when associated with MiniVs (51 vs. 22%, *n* = 3). **(I)** Left: Quantification (%) of 15-min SAg-specific conjugates harboring CD3ζ staining at the IS (≥50 cells/sample, *n* = 3, one-way ANOVA test; ****, P ≤ 0.0001; **, P ≤ 0.01; *, P ≤ 0.05). Right: Relative CD3ζ fluorescence intensity at the IS (recruitment index; 10 cells/sample, *n* = 3, Kruskal–Wallis test; ****, P ≤ 0.0001). Nonsignificant differences are not shown. Source data are available for this figure: SourceData F1.

lack of effect of Spike, despite the overall impairment in TCR signaling. However, LAMP1 staining was distributed over the entire plasma membrane in SAg-specific conjugates formed using Spike W–pretreated CTLs, as opposed to the respective control conjugates, where LAMP1 staining was selectively concentrated at the IS (Fig. 3 F). No LAMP1 staining was detectable in the absence of SAg (Fig. 3 F). Hence, Spike pretreatment results in the failure of CTLs to undergo polarized degranulation.

We previously reported that polarized degranulation by CTLs is essential for target cell killing (Kabanova et al., 2016), suggesting that Spike may suppress CTL-mediated cytotoxicity. To address this possibility, we carried out fluorimetry-based cytotoxicity assays by incubating Spike W–pretreated CTLs with SAg-pulsed Raji cells loaded with calcein AM, a cell-permeant dye that becomes fluorescent following hydrolyzation by intracellular esterases and is released by dying cells (Kummerow et al., 2014). Consistent with the defect in LG release at the IS, a time course analysis of fluorescent calcein release by target cells showed that Spike W suppressed the ability of CTLs to kill target cells at all effector:target (E:T) cell ratios tested (Fig. 3 G) and in a dose-dependent manner (Fig. S1 G). Similar results were obtained in an antigen-specific system using melanoma-specific CTLs generated from melanoma patients as CTLs and the HLA-matched melanoma cell line A375 as the target cells. For these experiments, CTLs were pretreated with Spike W or MiniVs, and target cell killing was measured 18 h later by flow cytometry after staining with propidium iodide (Fig. 3, H and I).

To further confirm the inhibitory effect of Spike on CTL-mediated killing, we generated an A375 cell transfectant overexpressing Spike W and an empty vector control transfectant and tested their ability to affect CTL function. Spike-overexpressing melanoma cells recapitulated the suppressive effects of Spike pretreatment on CTL cytotoxicity (Fig. 3 J). Hence, Spike W prevents CTLs from forming functional immune synapses, which results in impaired LG polarization to and release at the IS, thereby compromising their killing potential.

To understand whether Spike impairs CTL function beyond cytotoxicity, we assessed their ability to produce cytokines using IFNγ as a readout. IFNγ quantification in the supernatants of melanoma-specific CTLs activated by autologous B cells pulsed with the melanoma antigen MAGE A3 36 h after conjugate formation showed a reduction in IFNγ production by CTLs pretreated with soluble Spike (Fig. S1 H and Fig. S2 A) or MiniVs (Fig. S2 B). Similar results were obtained when melanoma-specific CTLs were mixed with Spike-overexpressing A375 cells (Fig. S2 C), indicating that Spike elicits long-lasting inhibitory effects on CTLs.

The inhibitory effects of Spike on IS formation are mediated by ACE2 and can be detected in acutely infected SARS-CoV-2 patients

To achieve insights into the mechanism underlying the suppressive activity of Spike on CTL IS assembly and function, we extended the analysis to the Spike variants Omicron BA.1 and BA.2. These variants recapitulated the effects of Spike W on IS assembly, as assessed by measuring the synaptic accumulation of tyrosine phosphoproteins and TCR/CD3 complexes (Fig. 4, A and B), as well as centrosome polarization toward the IS (Fig. 4 C). Since the mutations carried by the Omicron Spike variants do not compromise ACE2 binding (Wrapp et al., 2020; Yin et al., 2022), this result suggests that the effects of Spike on CTLs are mediated by ACE2. Consistent with this notion, pretreatment of CTLs with Spike W or Spike Omicron BA.1 in the presence of specific neutralizing mAbs that prevent Spike binding to ACE2 (Andreano et al., 2021a; Andreano et al., 2021b; Torres et al., 2022) reverted the suppressive effects of the Spike variants on IS assembly by CTLs (Fig. 4, A–D).

To further address the role of ACE2 in Spike-mediated CTL suppression, we investigated the outcome of Spike treatment in freshly purified, quiescent $CD8^+$ T cells, which do not express ACE2 (Fig. 1 A). Spike did not affect IS assembly in these cells (Fig. S2, D–F). However, ACE2 overexpression made quiescent $CD8^+$ T cells responsive to Spike (Fig. 4, E and D). Hence, the inhibitory effects of Spike on IS formation are specifically mediated by ACE2.

To validate these results in the context of SARS-CoV-2 infection, we assessed the ability of CTLs naturally exposed to Spike in acutely infected patients to form functional immune synapses. Mononuclear cells from bronchoalveolar lavage (BAL) and matched peripheral blood lymphocytes (PBL) from three acutely infected patients, and control PBLs from healthy donors, were mixed with SAg-pulsed Raji cells and used to assess their ability to assemble functional immune synapses, as assessed by imaging tyrosine phosphoprotein accumulation at the APC contact. CTLs were discriminated against by the presence of LGs labeled with anti-GzmB mAb. BALs, but not PBLs, from these patients were found to display severe defects in IS signaling in the absence of exogenously added Spike that recapitulated those observed in healthy, Spike-treated CTLs (Fig. 4 F). Although other factors may contribute to this phenotype, these data strongly suggest that in vivo CTL exposure to Spike in the

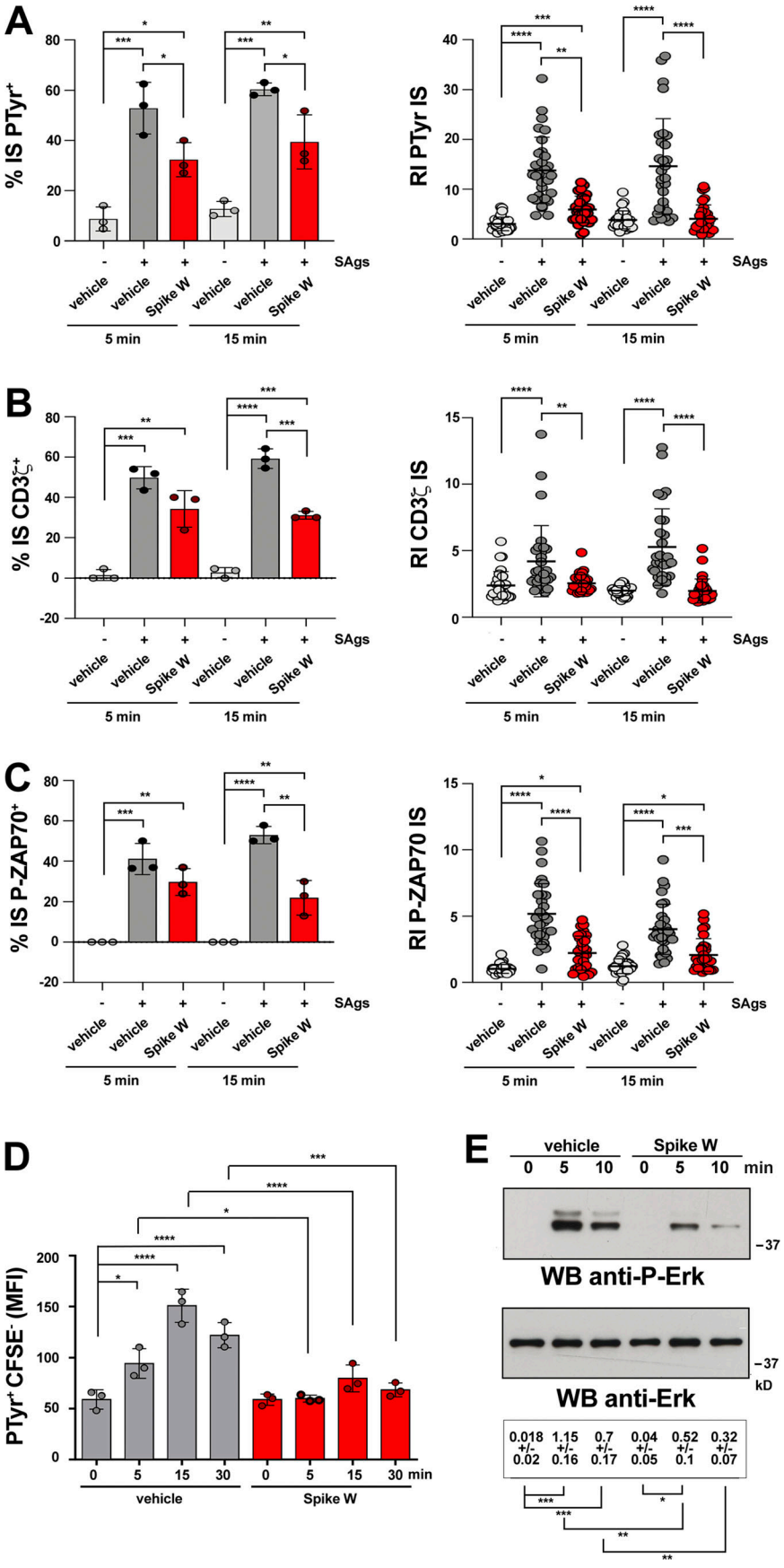

Figure 2. **Spike suppresses signaling at an early step of IS assembly. (A–C)** Left: Quantification (%) of 5-min and 15-min SAg-specific conjugates harboring PTyr (A), CD3ζ (B), or P-ZAP-70 (C) staining at the IS in CTLs (day 7) pretreated with either vehicle (PBS) or 0.05 µg/µl Spike W, then mixed with Raji cells (APCs) either unpulsed or pulsed with a combination of SEA, SEB, and SEE (SAgs), and incubated for 5 or 15 min at 37°C (≥50 cells/sample, *n* = 3, one-way ANOVA test; ****, P ≤ 0.0001; ***, P ≤ 0.001; **, P ≤ 0.01; *, P ≤ 0.05). Right: Relative PTyr (A), CD3ζ (B), or P-ZAP-70 (C) fluorescence intensity at the IS (recruitment index; 10 cells/sample, *n* = 3, Kruskal–Wallis test; ****, P ≤ 0.0001; ***, P ≤ 0.001; **, P ≤ 0.01; *, P ≤ 0.05). **(D)** Flow cytometric analysis of protein tyrosine phosphorylation in conjugates prepared as in A–C and incubated at 37°C for the indicated times. Raji cells were loaded with 1.5 µM CFSE prior to conjugate formation. Conjugates were stained with anti-PTyr mAb followed by fluorescently labeled secondary Abs. The analysis was carried out gating on $CFSE^-$ cells (*n* = 3, one-way ANOVA test; ****, P ≤ 0.0001; ***, P ≤ 0.001; *, P ≤ 0.05). **(E)** Immunoblot analysis of Erk phosphorylation in CTLs activated with anti-CD3 and anti-CD28 mAbs. CTLs were incubated at 37°C for the indicated times and processed for immunoblot with Abs against the active forms of Erk1/2. Stripped filters were blotted with anti-Erk2 mAb as loading control. The migration of molecular mass markers is indicated (*n* = 2, one-way ANOVA test; ***, P ≤ 0.001; **, P ≤ 0.01; *, P ≤ 0.05). Data are expressed as mean ± SD. ****, P ≤ 0.0001; ***, P ≤ 0.001; **, P ≤ 0.01; *, P ≤ 0.05. Nonsignificant differences are not shown. Source data are available for this figure: SourceData F2.

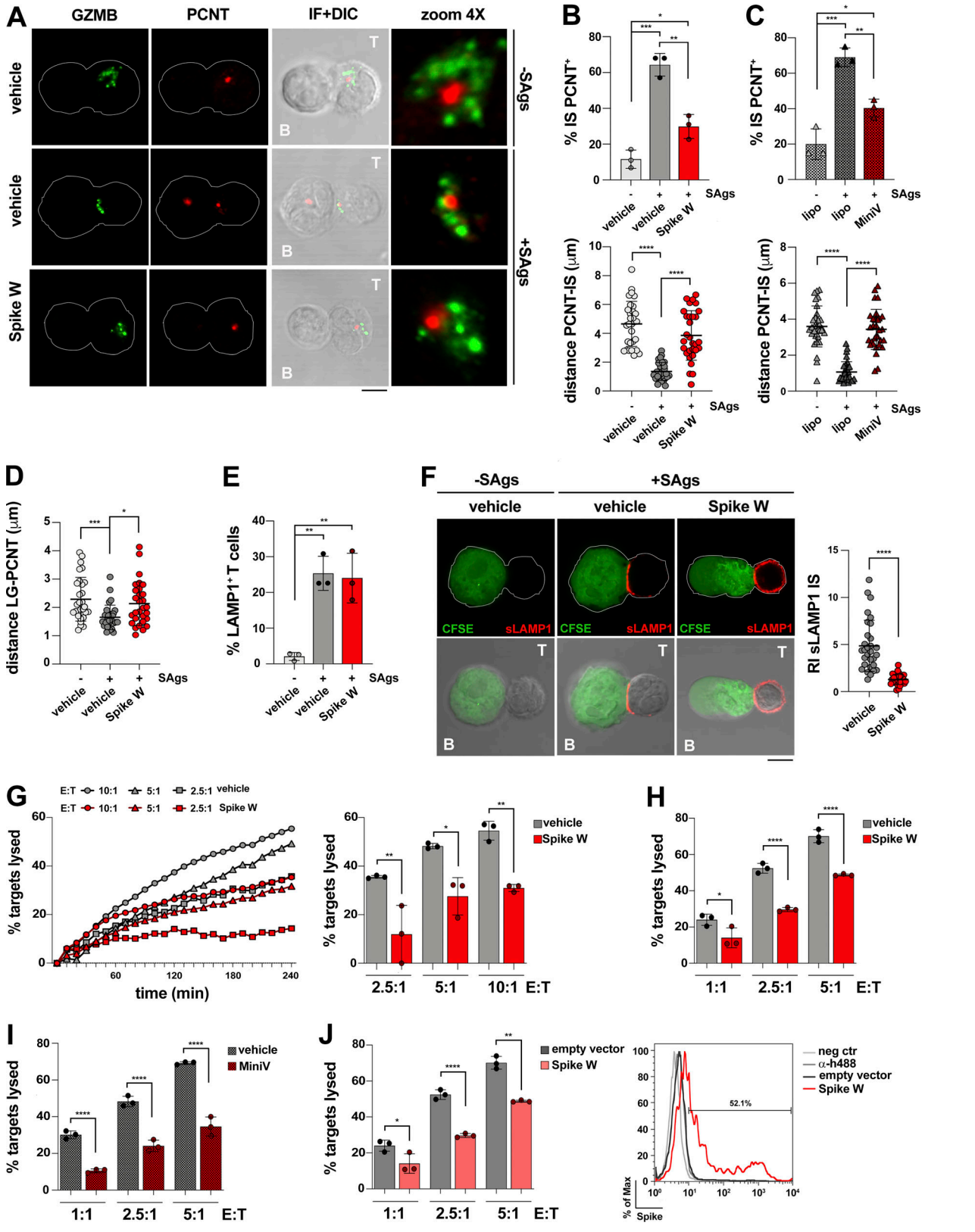

Figure 3. **Spike inhibits centrosome and LG polarization to the CTL IS and CTL-mediated cytotoxicity. (A–D)** Immunofluorescence analysis of PCNT and GrzmB in CTLs (day 7) pretreated with either vehicle (PBS) or 0.05 µg/µl Spike W (A, B, and D) or with 1.2 × 10^9 control liposomes or MiniVs (A–C), then mixed with Raji cells (APCs) either unpulsed or pulsed with a combination of SEA, SEB, and SEE (SAgs), and incubated for 15 min at 37°C. Representative images (medial optical sections) of the conjugates are shown (A). **(B and C)** Top: Quantification (%) of 15-min SAg-specific conjugates harboring PCNT staining at the IS (≥50 cells/sample, *n* = 3, one-way ANOVA test; ***, P ≤ 0.001; **, P ≤ 0.01; *, P ≤ 0.05). Bottom: Measurement of the distance (µm) of the centrosome (PCNT) from the CTL-APC contact site (10 cells/sample, *n* = 3, one-way ANOVA test; ****, P ≤ 0.0001). **(D)** Measurement of the distance (µm) of the LGs (marked by

GzmB) from the centrosome (PCNT) in conjugates formed with Spike W–pretreated CTLs (10 cells/sample, *n* = 3, Kruskal–Wallis test; ***, P ≤ 0.001; *, P ≤ 0.05; see Fig. S2 for parameters used for measurements plotted in B–D). **(E)** Flow cytometry analysis of degranulation of CTLs (day 7) pretreated with either vehicle (PBS) or Spike W and cocultured with CFSE-stained Raji cells loaded with SAg at an E:T cell ratio 2.5:1 for 1 h. The histogram shows the percentage (%) of LAMP1$^+$ T cells (*n* = 3, one-way ANOVA test; **, P ≤ 0.01). **(F)** Immunofluorescence analysis of degranulation of CTLs (day 7) pretreated with either vehicle (PBS) or Spike W and co-cultured with CFSE-stained Raji cells loaded with SAg at an E:T cell ratio 2.5:1 for 1 h. Conjugates were fixed and stained without prior permeabilization with anti-LAMP1 mAb and fluorescently labeled secondary Abs to detect plasma membrane–associated LAMP1. The histogram shows the relative surface LAMP1 fluorescence (sLAMP1) intensity at the IS (recruitment index) of SAg-specific conjugates in the absence or presence of Spike (10 cells/sample, *n* = 3, Kruskal–Wallis test; ****, P ≤ 0.0001). Negative control conjugates (no SAg) were not quantified as no sLAMP1 fluorescence was detectable. Representative images (medial optical sections) of the conjugates are shown. **(G)** Fluorimetric analysis of cytotoxicity of CTLs (day 7) using the calcein release assay. CTLs were pretreated with either vehicle (PBS) or Spike W and cocultured with SAg-pulsed, calcein AM–loaded Raji cells at different E:T cell ratios for 4 h. The representative curves show the kinetics of target cell lysis by CTLs at the indicated E:T cell ratios. The histogram shows the target cell lysis at 4 h (*n* = 3, one-way ANOVA test; **, P ≤ 0.01; *, P ≤ 0.05). **(H and I)** Flow cytometric analysis of antigen-specific target cell killing by melanoma-specific CTLs derived from three patients, pretreated with either vehicle (PBS) or Spike W, or with 1.2 × 10^9 control liposomes or MiniVs, using as target the melanoma cell line A375. Cells were cocultured for 18 h and stained with propidium iodide and anti-CD8 mAb prior to processing for flow cytometry. Analyses were carried out gating on CD8$^-$/PI$^+$ cells. The histograms show the percentage (%) of target cells lysed (*n* = 3, one-way ANOVA test; ****, P ≤ 0.0001; *, P ≤ 0.05). **(J)** Flow cytometric analysis of antigen-specific target cell killing by melanoma-specific CTLs derived from three patients, using as target A375 melanoma cells transiently transfected with either a construct encoding Spike W or the empty control vector (54.0 ± 1.7% transfected cells, as assessed by flow cytometric analysis with anti-Spike mAb J08; representative flow cytometric data are shown). Cells were co-cultured for 18 h and processed as in I. The histograms show the percentage (%) of target cells lysed (*n* = 3, one-way ANOVA test; ****, P ≤ 0.0001; **, P ≤ 0.01; *, P ≤ 0.05). Data are expressed as mean ± SD. Scale bar, 5 µm. Nonsignificant differences are not shown.

respiratory tract during acute infection compromises their ability to form functional immune synapses.

ACE2 engagement impairs CTL IS formation and cytotoxicity

ACE2 is a type I transmembrane zinc metalloprotease that plays a key role in the renin–angiotensin system (RAS). The extracellular carboxypeptidase domain of ACE2 catalyzes the conversion of angiotensin (Ang) I to Ang (1-9), and Ang II and Ang (1-9) to the bioactive peptide Ang (1-7), which activates the receptor MAS1 on the target cells (Samavati and Uhal, 2020). However, ACE2 also acts as a receptor that modulates intracellular processes in a peptidase-independent manner through distinct contributions of its extracellular, transmembrane, and intracellular domains, including integrin transactivation, regulation of amino acid transporters, and endocytosis-dependent infection by SARS-CoV-2 (Danilczyk et al., 2006; Hoffmann et al., 2020; Inoue et al., 2007; Simons et al., 2021). To address how ACE2 mediates the suppressive effects of Spike on IS formation, we first investigated the localization of ACE2 in SAg-specific conjugates using CD8$^+$ T cells transfected with an ACE2-GFP encoding construct or control GFP-encoding vector. ACE2 was found to accumulate at the IS in the absence of the Spike (Fig. 5 A). Interestingly, ACE2 recruitment to the IS was impaired in the presence of Spike (Fig. 5 A), suggesting that ACE2 ligands may modulate IS assembly by preventing their correct localization.

We next assessed the outcome of ACE2 engagement on IS assembly in CTLs using as the ligand an anti-ACE2 polyclonal Ab raised against the extracellular domain that blocks SARS-CoV-2 entry into target cells by competing with Spike for ACE2 binding (Hoffmann et al., 2020). CTL pretreatment with the anti-ACE2 Ab recapitulated the suppressive effects of Spike on IS assembly, including the synaptic accumulation of tyrosine phosphoproteins and TCR/CD3 complexes (Fig. 5, B and C), centrosome polarization toward the IS (Fig. 5 D), and LG convergence toward the centrosome (Fig. 5 E). Consistently, CTL-mediated killing (Fig. 5, F and G) and IFNγ production (Fig. S3 A) were suppressed under these conditions. Similar to Spike, the anti-ACE2 Ab suppressed the formation of signaling-competent immune synapses in CTLs at an early maturation step, as assessed by analyzing immune synapses formed in 5-min versus 15-min CTL-target cell conjugates (Fig. S3, B–D). No effect on IS assembly was observed when freshly purified CD8$^+$ T, which do not express ACE2 (Fig. 1 A), were pretreated with the anti-ACE2 Ab (Fig. S3, E–G). Of note, while angiotensin II (Ang II) suppressed the assembly of functional immune synapses in CTLs, similar to the anti-ACE2 Ab, no effect was observed when cells were treated with Ang (1-7; Fig. 5, B–E), ruling out the catalytic activity of ACE2 in this function as well as indirect effects mediated by the Ang (1-7) receptor MAS1. Of note, while MAS1 was expressed in the CD8$^+$ T cell, its expression decreased during their differentiation to CTLs (Fig. S3 H). Taken together, these results support the notion that following ligand binding, ACE2 delivers inhibitory signals to suppress IS assembly.

Collectively, our results provide novel insights into the mechanisms of immune evasion by SARS-CoV-2, involving the Spike-ACE2 axis, as a means for infected cells to avoid killing. We believe that the effects that we observed in vitro can be related to the physiological setting of SARS-CoV-2 infection, as strongly supported by the IS defects in CTLs from acutely infected patients. Of note, it has been calculated that during infection, in vivo individuals carry up to 10^{11} virions/ml in the sputum (Bar-On et al., 2020) or 10^{11} virions in the lungs (Sender et al., 2021), which translates into ∼4 µg of Spike protein, an amount that is in the range of the one we used in vitro. Given that the virus multiplies at the epithelial level, we believe that the local concentration of the Spike may easily exceed the levels used in our in vitro experiments. In addition, while soluble Spike was able to suppress CTL IS assembly and cytotoxicity, each virus displays ∼60 copies of the Spike trimer on its surface, which is likely to amplify signaling through receptor clustering. In support of this notion, MiniVs, which carry ∼18–40 copies of trimeric Spike (Staufer et al., 2022), suppressed IS assembly and the function of CTLs at a concentration >twofold lower than soluble trimeric Spike (legend to Fig. 1 H).

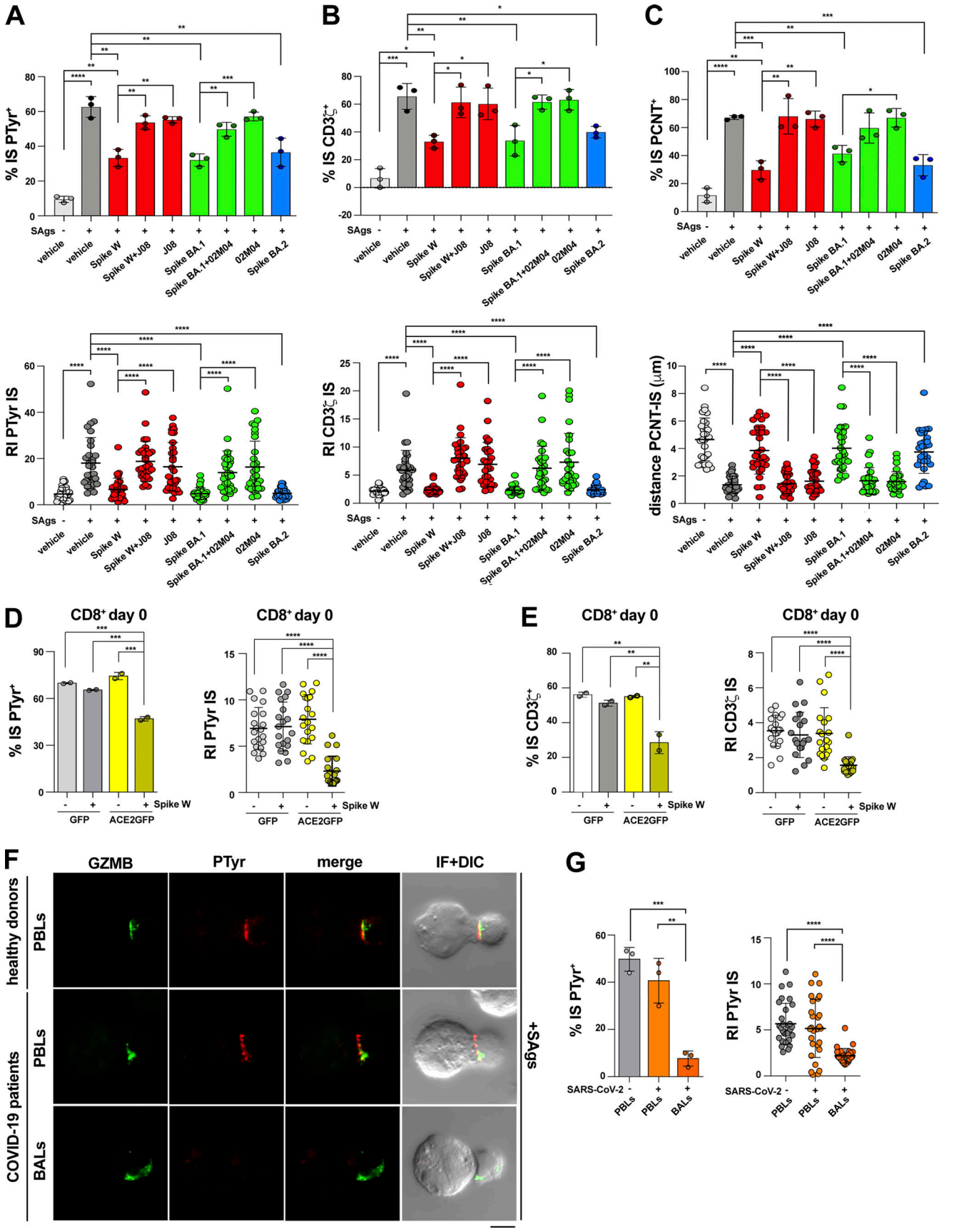

Figure 4. **The inhibitory effects of Spike on IS formation are mediated by ACE2 and can be detected in acutely infected SARS-CoV-2 patients. (A and B)** Top: Quantification (%) of 15-min antigen-specific conjugates harboring PTyr (A) or CD3ζ (B) staining at the IS in CTLs (day 7) pretreated with either

vehicle (PBS) or 0.05 µg/µl Spike W, Spike Omicron BA.1 (Spike BA.1), alone or in the presence of the respective neutralizing mAb (Spike W + J08; Spike BA.1 + 02M04); or Spike Omicron BA.2 (Spike BA.2). Samples pretreated with only the neutralizing mAbs (J08 and 02M04) were also included in the analysis. CTLs were mixed with Raji cells (APCs), either unpulsed or pulsed with a combination of SEA, SEB, and SEE (SAgs), and incubated for 15 min at 37°C (≥50 cells/sample, n = 3, unpaired two-tailed Student's t test; ****, P ≤ 0.0001; ***, P ≤ 0.001; **, P ≤ 0.01; *, P ≤ 0.05). Bottom: Relative PTyr (A) or CD3ζ (B) fluorescence intensity at the IS (recruitment index; 10 cells/sample, n = 3, Kruskal–Wallis test; ****, P ≤ 0.0001). **(C)** Top: Quantification (%) of 15-min antigen-specific conjugates formed as in panel A harboring PCTN1 staining at the IS (≥50 cells/sample, n = 3, one-way ANOVA test; ****, P ≤ 0.0001; ***, P ≤ 0.001; **, P ≤ 0.01; *, P ≤ 0.05). Bottom: Measurement of the distance (µm) of the centrosome (PCNT) from the T cell–APC contact site (10 cells/sample, n = 3, Kruskal–Wallis test; ****, P ≤ 0.0001). **(D and E)** Immunofluorescence analysis of PTyr (D) and CD3ζ (E) in purified CD8⁺ T cells transfected with an ACE2-GFP–expressing construct or empty vector, pretreated with either vehicle (PBS) or 0.05 µg/µl Spike W, then mixed with Raji cells (APCs) either unpulsed or pulsed with a combination of SEA, SEB, and SEE (SAgs), and incubated for 15 min at 37°C. The histograms show (left) the quantification (%) of conjugates harboring PTyr (D) and CD3ζ (E) staining at the IS (top; ≥50 cells/sample, n = 2, one-way ANOVA test; ***, P ≤ 0.001; **, P ≤ 0.01), or (right) the relative PTyr (D) and CD3ζ (E) fluorescence intensity at the IS (recruitment index; 10 cells/sample, n = 2, Kruskal–Wallis test; ****, P ≤ 0.0001). Quantification was carried out on GFP⁺ cells. **(F)** Immunofluorescence analysis of PTyr and GrzB in BALs or PBLs from patients with acute SARS-CoV-2 infection, or PBLs from healthy donors, mixed with Raji cells (APCs) pulsed with a combination of SEA, SEB, and SEE (SAgs), and incubated for 15 min at 37°C. Representative images (medial optical sections) of the T cell:APC conjugates are shown. **(G)** The histograms show (left) the quantification (%) of 15-min SAg-specific conjugates harboring PTyr staining at the IS (≥50 cells/sample, n = 3, one-way ANOVA test; ***, P ≤ 0.001; **, P ≤ 0.01), or (right) the relative PTyr fluorescence intensity at the IS (recruitment index; 10 cells/sample, n = 3, Kruskal–Wallis test; ****, P ≤ 0.0001). The analysis was restricted to CTLs, identified by GrzB staining. Data are expressed as mean ± SD. Nonsignificant differences are not shown. Scale bar, 5 µm.

The mechanism underlying the inhibitory effects of Spike on IS assembly remains to be elucidated. Our data show that SARS-CoV-2 Spike protein binding to ACE2 interferes with the assembly of a functional IS in CTLs by inhibiting the process at an early step, concomitant with ACE2 exclusion from the IS. Potential targets of the ACE2-Spike axis are integrins, such as LFA-1, which are essential for the generation of well-structured immune synapses characterized by the tight accumulation of TCR/CD3 complexes at the center of the contact area with the APC (Cassioli et al., 2021a). ACE2 has been reported to constitutively interact with β1 and α5 integrins, promoting cell adhesion and modulating downstream signaling (Clarke et al., 2012; Lin et al., 2004). Whether ACE2 binds to and modulates signaling by T cell integrins is as yet an open question. The finding that ACE2 is recruited to the IS and fails to do so when engaged by ligand suggests the intriguing possibility that, in the absence of ligand, ACE2 may contribute to IS assembly by promoting integrin-dependent adhesion.

It is noteworthy that, close to the ACE2 binding site, Spike displays a conserved RGD sequence, the consensus integrin-binding motif (Sigrist et al., 2013). Experimental evidence supports the notion that β1 and αv integrins may act as alternative Spike receptors or coreceptors together with ACE2 (Norris et al., 2022 *Preprint*; Park et al., 2021). Mechanistically, Spike has been shown to modulate β1 integrin signaling in the kidney cell line Vero E6 for productive infection by activating inside-out signaling mediated by Gα13 and adaptor talin (Simons et al., 2021). Additionally, the RGD sequence within the ACE2-binding domain of Spike has been recently identified as an αv-selective integrin agonist in primary human airway epithelial cells, where it triggers cell spreading, formation of focal adhesions, and actin reorganization through the activation of the kinases FAK and Src, and the adaptor paxillin (Norris et al., 2022 *Preprint*). However, the fact that integrin activation is a key activating event required for the onset of IS assembly (Springer and Dustin, 2012) and that Spike suppresses this process strongly suggests that the inhibitory effects of Spike on the CTL IS are not mediated by integrins. Additionally, our data show that the Spike Omicron BA.2 variant, which carries a nonconservative D to N substitution at position 405 of the RGD integrin-binding motif mapping at positions 403–405 (RGN), is as effective as Spike W and Spike Omicron BA.1 at suppressing IS assembly. Conversely, the ability of mAbs that prevents Spike binding to ACE2, together with the lack of any effect of Spike on IS assembly in freshly purified CD8⁺ T cells that do not express ACE2 but their acquired susceptibility to Spike following forced ACE2 expression, highlights the key role of ACE2 in the Spike-dependent suppression of IS assembly and CTL-mediated killing.

While the role of ACE2 as an ectoenzyme that participates in the RAS has been extensively characterized, the role of its transmembrane and intracellular domains, which together display 48% identity with collectrin (Zhang et al., 2001), is only beginning to be explored. Both domains have been implicated in SARS-CoV-2 infection through the endocytic uptake of the virus following Spike-mediated binding to the extracellular domain of ACE2 (Hoffmann et al., 2020; Inoue et al., 2007). Additionally, the collectrin homology domain has been shown to act as a chaperone to stabilize transporters of large neutral amino acids at the surface of intestinal epithelial cells to regulate amino acid absorption (Camargo et al., 2009; Kowalczuk et al., 2008). The intracellular domain also regulates the TACE/ADAM17-mediated shedding of the extracellular domain to its catalytically active soluble form by interacting with calmodulin (Lambert et al., 2008). Of note, CTLs could become susceptible to SARS-CoV-2 infection as a result of ACE2 expression, and indeed, this possibility has been proven in total activated peripheral T cells (Welch et al., 2022), suggesting that CTLs might first be disabled by Spike targeting of the IS and then killed by CTLs newly recruited to the site of infection.

The inhibitory effects of ACE2 ligands, but not of the product of its catalytic activity Ang(1-7), on TCR signaling and IS assembly support the notion that ACE2 limits CTL activation in a peptidase-independent fashion through signals triggered in response to ligand binding. Since anti-ACE2 Abs have been shown to be effective in limiting SARS-CoV-2 production in cellular and animal models (Chen et al., 2021; Chaouat et al., 2022), our findings raise the possibility that using these Abs as therapeutics

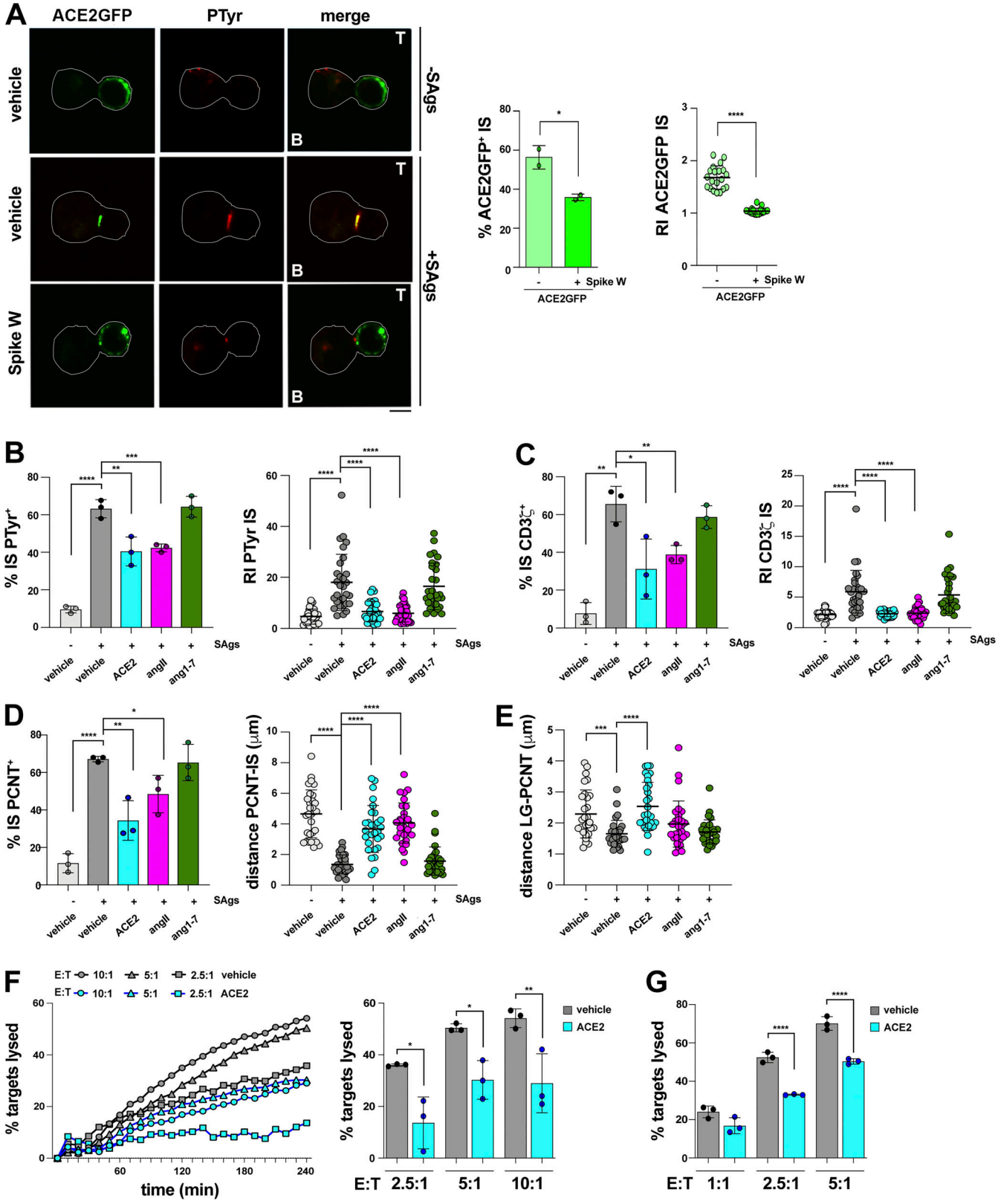

Figure 5. **ACE2 is recruited to the CTL IS and suppresses IS formation and cytotoxicity. (A)** Immunofluorescence analysis of ACE2 localization in purified CD8⁺ T cells transfected with an ACE2-GFP–expressing construct or empty GFP vector, pretreated with either vehicle (PBS) or 0.05 µg/µl Spike W, then mixed with Raji cells (APCs) either unpulsed or pulsed with a combination of SEA, SEB, and SEE (SAgs), and incubated for 15 min at 37°C. Representative images are shown. The histograms show (left) the quantification (%) of conjugates harboring ACE2-GFP staining at the IS (≥50 cells/sample, $n = 2$, one-way ANOVA test; *, $P \leq 0.05$), or (right) the relative ACE2-GFP fluorescence intensity at the IS (recruitment index; 10 cells/sample, $n = 2$, Kruskal–Wallis test; ****, $P \leq 0.0001$). **(B and C)** Left: Quantification (%) of 15-min conjugates harboring PTyr (B) or CD3ζ (C) staining at the IS. CTLs (day 7) were conjugated with Raji cells (APCs) in

the absence or presence of SAgs and either an anti-ACE2 Ab (cell viability after pretreatment 93.7 ± 0.8%), or Ang II, or the peptide Ang 1-7 (≥50 cells/sample, *n* = 3, one-way ANOVA test; ****, P ≤ 0.0001; ***, P ≤ 0.001; **, P ≤ 0.01; *, P ≤ 0.05). Right: Relative PTyr (B) or CD3ζ (C) fluorescence intensity at the IS (recruitment index; 10 cells/sample, *n* = 3, Kruskal–Wallis test; ****, P ≤ 0.0001). **(D)** Left: Quantification (%) of 15-min conjugates formed as in A harboring PCTN staining at the IS (≥50 cells/sample, *n* = 3, one-way ANOVA test; ****, P ≤ 0.0001; **, P ≤ 0.01; *, P ≤ 0.05). Right: Measurement of the distance (µm) of the centrosome (PCNT) from the T cell–APC contact site in CTL-APC conjugates formed as in A (10 cells/sample, *n* = 3, Kruskal–Wallis test; ****, P ≤ 0.0001). **(E)** Measurement of the distance (µm) of the LGs (marked by GzmB) from the centrosome (PCNT) in 15-min CTL-APC conjugates formed as in A (10 cells/sample, n = 3, Kruskal–Wallis test; ****, P ≤ 0.0001; ***, P ≤ 0.001). **(F)** Fluorimetric analysis of cytotoxicity of CTLs (day 7) using the calcein release assay. CTLs were pretreated with either vehicle (PBS) or 2 µg/ml anti-ACE2 Ab (ACE2) and co-cultured with SAg-pulsed, calcein AM–loaded Raji cells at different E:T cell ratios for 4 h. The representative curves show the kinetics of target cell lysis by CTLs at the indicated E:T cell ratios. The histogram shows the target cell lysis at 4 h (*n* = 3, one-way ANOVA test; **, P ≤ 0.01; *, P ≤ 0.05). **(G)** Flow cytometric analysis of antigen-specific target cell killing by melanoma-specific CTLs derived from three patients, using as target the melanoma cell line A375. CTLs were pretreated as in F, cocultured with A375 cells for 18 h, and processed for flow cytometry after staining with propidium iodide and anti-CD8 mAb. Analyses were carried out gating on $CD8^-/PI^+$ cells. The histograms show the percentage (%) of target cells lysed (*n* = 3, one-way ANOVA test; ****, P ≤ 0.0001). The data are expressed as mean ± SD. Nonsignificant differences are not shown. Scale bar, 5 µm.

in COVID-19 patients may lead to unwanted immune suppression.

It is noteworthy that a functional RAS has been documented in T cells (Coppo et al., 2011). Among the RAS components, the Ang II receptor AT1 has been reported to have immunomodulatory effects on T cells, limiting harmful $CD8^+$ T cell responses during blood-stage malaria and promoting a protective $CD4^+$ T cell response in the kidney in the setting of hypertension (Silva-Filho et al., 2016; Silva-Filho et al., 2017; Zhang et al., 2012). This suggests that ACE2 may participate in T cell immunity through both its enzyme-independent and its enzyme-dependent activities.

Other viruses have co-opted the T cell IS as a target to escape immunosurveillance. One of the most striking examples is HIV-1, which exploits the virulence factor Nef to subvert the process of vesicular trafficking required for the coordinated transport of key signaling components to the IS, leading to a nonproductive T cell response against the virus (Fackler et al., 2007). Importantly, the IS acts as a signaling and a cell–cell communication platform also for other immune cells, including helper T cells and B cells (Batista et al., 2001; Chemin et al., 2012; Papa and Vinuesa, 2018). The data reported here highlight the intriguing possibility that SARS-CoV-2 may co-opt IS targeting as a wide-ranging immunomodulatory strategy, beyond the suppression of CTL function, to evade the adaptive immune response of the host.

Materials and methods

Cells, plasmids, and Abs

Peripheral blood and BAL samples were obtained after informed consent according to the Declaration of Helsinki. Experiments were performed after approval by the local ethics committee (Comitato Etico Regione Toscana Area Vasta Sud Est and Area Vasta Centro).

Primary human $CD8^+$ T cells were isolated from buffy coats of healthy donors and purified (>95%) by negative selection using the RosetteSep Human $CD8^+$ T Cell Enrichment Cocktail (#15063; StemCell Technologies), according to the manufacturer's instructions. $CD8^+$ T cells were cultured immediately following isolation at 37°C and 5% CO_2 in RPMI-HEPES medium (#R7388; Merck) supplemented with 10% iron-enriched bovine calf serum (BCS; #SH30072.03; GE Healthcare HyClone) and 1% MEM nonessential amino acids (MEM NEAA; #11140050) at a density of 1×10^6/ml.

Melanoma-specific $CD8^+$ T cells were derived from the peripheral blood of three melanoma HLA $A02^+$/HLA $A24^+$ patients. Briefly, peripheral blood mononuclear cells were isolated by Ficoll-Hypaque density gradient centrifugation (Lymphoprep, Alere Technologies). A portion of them was frozen in DMSO 10% at −80°C for future use as APCs. The remaining part was incubated with CD8 MicroBeads for the MACS cell separation method (Miltenyi Biotec, https://www.miltenyibiotec.com/IT-en/products/macs-cell-separation.html). $CD8^+$ T cells purified from donors, according to the manufacturer's protocol, were cocultured with 1×10^6 irradiated A375 melanoma cells (ATCC) and 0.5×10^6 irradiated autologous APCs in RPMI 1640 complete medium to obtain $CD8^+$ cell lines specific for A375 melanoma cells. After 10 d of coculture, the CTLs were analyzed for their responsiveness to melanoma A375 and MAGE A3 antigens by measuring $[^3H]$-thymidine uptake (D'Elios et al., 1997).

BAL samples from severely affected SARS-CoV-2 patients were collected and layered on Ficoll-Hypaque density gradient to isolate BAL-derived T cells, as described (Amedei et al., 2009). PBL were isolated from the same patients as well as from healthy donors by Ficoll-Hypaque density gradient.

The Burkitt lymphoma–derived B cell line Raji was grown at 37°C and 5% CO_2 in RPMI-1640 medium (#R8758; Merck) supplemented with 7.5% BCS. The melanoma line A375 (ATCC) was grown in DMEM High Glucose (#ECB7501L; EuroClone) supplemented with 10% FCS. To investigate the effects of cell-bound Spike on CTL function, a Spike-overexpressing A375 transfectant was generated with a Spike W–encoding pcDNA3 construct. Cells were transfected using the Turbofect transfection reagent (Thermo Fisher Scientific) and tested after 24 h for Spike expression at the plasma membrane by flow cytometry. An empty vector transfectant was generated as the negative control.

Plasmids included pcDNA3 (Thermo Fisher Scientific), pcDNA3-Spike W (#145032; Addgene), and pcDNA3-ACE2-GFP (#154962; Addgene). The Wuhan Spike protein was generated using a plasmid encoding the SARS-CoV-2 S-2P construct (Wrapp et al., 2020). The Omicron BA.1 Spike protein was generated using the SARS-CoV-2 S HexaPro construct (ID: 154754; Addgene) containing the Spike sequence of this variant.

Primary commercial Abs used in this work for immunofluorescence analysis were from SantaCruz (CD3ζ, clone 6B10.2, #sc-1239), Cell Signaling (P-ZAP-70 Y319/ Syk Y352, #2701S; PTyr, #8954S), Abcam (PCNT, #4448), BD Biosciences (Granzyme B, #560211), and BioLegend (APC anti-human CD107a/LAMP1, #328619). Alexa Fluor 488-, 555-, and 647-labeled secondary Abs were from Thermo Fisher Scientific (anti-mouse 488, #A11001; anti-mouse 555, #21422; anti-rabbit 555, #A21428; anti-rabbit 647, #A21244).

SARS-CoV-2 Spike protein expression and purification

Plasmids encoding the Spike W and Spike Omicron BA.1 and BA.2 were transiently transfected in Expi293F cells and ExpiCHO-S cells (Thermo Fisher Scientific), respectively. Cells were grown for 6 d at 37°C with 8% CO_2 shaking at 125 rpm according to the manufacturer's protocol (Thermo Fisher Scientific). Cell cultures for Spike W and Spike Omicron BA.1 and BA.2 were harvested 6 d after transfection. Collected supernatants were clarified by centrifugation (1,200 ×*g*, 30 min, 4°C) followed by filtration through a 0.45 µm filter. Chromatography purification was conducted at room temperature using ÄKTA Go purifier system from GE Healthcare Life Sciences. Filtrated culture supernatants were purified with a 5 ml HisTrap FF Crude column (GE Healthcare Life Sciences), previously equilibrated in Buffer A (20 mM NaH_2PO_4, 500 mM NaCl + 30 mM Imidazol pH 7.4). Spike proteins were eluted from the column with five column volumes of 60% Buffer B (20 mM NaH_2PO_4, 500 mM NaCl + 500 mM Imidazol pH 7.4). Eluted fractions were pooled and dialyzed with PBS buffer pH 7.4 using Slide-A-Lyzer Dialysis Cassette 10 K molecular weight cutoff (Thermo Fisher Scientific) overnight at 4°C. The final Spike protein concentration was determined by measuring the absorbance at 562 nm using Pierce BCA Protein Assay Kit (Thermo Fisher Scientific). Final proteins were dispensed in aliquots of 0.5 ml each and stored at −80°C prior to use.

Minimal SARS-CoV-2 virions (MiniVs)

Synthetic virions were formed as described previously (Staufer et al., 2022). Briefly, liposomes were produced with a composition of 45 mol% 1,2-dioleoyl-sn-glycero-3-phosphocholine, 21 mol% 1,2-dioleoyl-sn-glycero-3-phosphoethanolamine, 3 mol% 1,2-dioleoyl-sn-glycero-3-phospho-L-serine, 12 mol% 1,2-dioleoyl-sn-glycero-3-phospho-(1′-myo-inositol), 14 mol% cholesterol, 3 mol % N-nervonoyl-D-erythro sphingosylphosphorylcholin, and 1 mol% DGS-NTA(Ni^{2+}) with a diameter of 108 ± 23 nm by extrusion in phosphate-buffered saline. All lipids were obtained from Avanti Polar Lipids. To image the localization and binding of the synthetic virions by fluorescence microscopy, 1 mol% fluorescent 1,2-dioleoyl-sn-glycero-3-phosphoethanolamine-N-(7-nitro-2-1,3-benzoxadiazol-4-yl)–labeled PE lipids were included in the initial lipid mixture used for liposome preparation. To form synthetic virions, recombinant histidine-tagged SARS-CoV-2 Spike protein (aa16-1213, RP-87671; Thermo Fisher Scientific) was conjugated to the liposomes to yield a final density of 18–40 Spike proteins per vesicle. Conjugation was performed for at least 20 min at 4°C in the dark. To analyze T cell–target cell synapse formation and cytotoxicity, the synthetic virions solution was diluted to a final particle concentration of 1.2 × 10^9/ml in the culture medium, which lies in the range of viral particle concentration found in the sputum of infected individuals (Bar-On et al., 2020). The final Spike concentration in this solution was 18 µg/ml.

Expression and purification of human anti-Spike mAbs

Expi293F cells (Thermo Fisher Scientific) were transfected with plasmids carrying J08 and 02M04Ab heavy and the light chains with a 1:2 ratio using ExpiFectamineTM293 Transfection Kit (Thermo Fisher Scientific) as recommended by the manufacturer. 3 and 6 d after transfection, cell cultures were harvested and clarified by centrifugation (1,100 ×*g* for 10 min at room temperature). Supernatants were recovered and filtered with a 0.45-µm filter to remove particulate material. The purification process was conducted at room temperature using the ÄKTA Go purification system (GE Healthcare Life Sciences) through a 1 ml HiTrap Protein G HP column (GE Healthcare Life Sciences), previously equilibrated with a loading buffer (0.02 M NaH2PO4 pH 7). Each mAb was eluted from the column in 1-ml fractions of elution buffer (0.1 M glycine-HCl, pH 2.7) and collected in vials predispensed with 100 µl of neutralization buffer (Tris-HCl pH 9.0). Protein-containing fractions were pooled and dialyzed in PBS 1× Buffer pH 7.4 with a 1:200 ratio using Slide-A-Lyzer Dialysis Cassettes, 10 K MWCO, 3 ml (Thermo Fisher Scientific) at 4°C overnight. The final Ab concentration was determined by measuring the absorbance at 562 nm using Pierce BCA Protein Assay Kit (Thermo Fisher Scientific). Purified Abs were stored at −80°C prior to use.

Spike binding assays

To analyze the binding of Spike protein to CTLs, 0.15 × 10^6 freshly purified $CD8^+$ T cells (day 0) and CTLs (day 7) were pretreated with Spike W, as described in "CTL pretreatments." Cells were then labeled with anti-Spike human J08 mAb for 30 min on ice. After washing with cold PBS, samples were incubated for 30 min on ice with Alexa Fluor 488–anti-human (#A11013; Thermo Fisher Scientific) secondary Ab and then analyzed by confocal microscopy. Alternatively, 0.15 × 10^6 CTLs (day 7) were incubated with MiniV or control liposomes as described in "CTL pretreatments" and analyzed by confocal microscopy.

CTL differentiation

$CD8^+$ T cells (1 × 10^6/ml) were stimulated and expanded in RPMI-HEPES supplemented with 10% BCS, 1% MEM NEAA, and 50 U/ml recombinant human IL-2 (#130-097-745; Miltenyi) with Dynabeads Human T-activator CD3/CD28 (#11132D; Gibco) the same day of the purification (day 0, also referred as resting $CD8^+$ T cells). After 48 h of activation (day 2), the beads were removed and the cells expanded in RPMI-HEPES supplemented with 10% BCS, 1% MEM NEAA, and 50 U/ml recombinant human IL-2 for another 3 d (day 5). 5 d after purification, the cells were further expanded for 2 d and collected on day 7.

CTL pretreatments

To allow for Spike binding on the cell surface, $CD8^+$ T cells (0.5 × 10^6) were incubated for 30 min at 20°C in 50 µl RPMI-HEPES in

the absence of BCS with 2.5 µg Spike W/BA.1/BA.2 or PBS vehicle control (concentration of Spike treatment chosen based on a dose-response analysis; see Fig. S2 B). Alternatively, CTLs were pretreated under the same conditions with 1.2 × 10^9/ml MiniVs or control liposomes. Spike W and the Omicron BA.1 variant were also incubated in combination with the respective neutralizing mAbs (J08 and 02M04, respectively) at a 1:3 protein:Ab ratio. Alternatively, CD8⁺ T cells (0.5 × 10^6) were incubated for 30 min at 20°C in 50 µl RPMI-HEPES in the absence of BCS with 2 µg/ml anti-ACE2 Ab (#AF933; R&D Systems; Hoffmann et al., 2020), the ACE2 substrate/ligand angiotensin II (#A9525; 1 µM; Merck), or the ACE2 product Ang (1-7; #A9202; 1 µM; Sigma-Aldrich).

For cytotoxicity assays, cells were pretreated in the same conditions in serum-free AIM V medium (#12055-091; calcein release assays; Gibco) or RPMI 1640 (flow cytometry–based assays). None of the treatments affected cell viability at the concentrations and times chosen for the analyses, as assessed by Trypan blue (T8154; Sigma-Aldrich) exclusion (see legends to Figs. 3 and 5).

CD8⁺ T cell transfections

Freshly purified CD8⁺ T cells were transiently transfected with the ACE2-GFP construct or GFP vector control (DNA/cells ratio = 1 µg/10^6 cells) using the Human T cell Nucleofector Kit (#VPA-1002; Amaxa Biosystem) and the Amaxa Nucleofector II system (Lonza), Program T-023. Cells were conjugated with SAg-loaded Raji cells 24 h after transfection.

Conjugate formation, immunofluorescence microscopy, and analysis

Conjugates between CD8⁺ T cells and superantigen-pulsed Raji B cells were carried out as previously described (Cassioli et al., 2021b). Raji B cells (0.08 × 10^6), used as APCs, were loaded with 10 µg/ml Staphylococcal superantigens A (SEA; #AT101; Toxin Technologies), B (SEB; #BT202; Toxin Technologies), and E (SEE; #ET404; Toxin Technologies) for 2 h and labeled with 10 µM Cell Tracker Blue for the last 15 min of incubation with the superantigens (+SAgs). The mix of SAgs was used to cover a substantial proportion of the TCR Vβ repertoire. Conjugates of CD8⁺ T cells with Raji B cells formed in the absence of SAgs were used as negative controls (–SAgs). Raji B cells, pulsed or not with SAgs, were washed twice, mixed with CD8⁺ T cells (0.12 × 10^6) pretreated as described above, and incubated for 15 min at 37°C. The same conditions were used for IS experiments on BALs and PBLs from acutely infected COVID-19 patients, using as positive controls PBLs from healthy donors. To analyze early TCR signaling events a shorter time of incubation (5 min) was included.

Samples for immunofluorescence analysis were seeded onto poly-L-lysine (#P1274; Merck)–coated slides (#X2XER208B; Thermo Fisher Scientific), fixed, and permeabilized for 10 min in methanol at −20°C (for CD3ζ and PTyr staining) or fixed for 15 min with 4% paraformaldehyde (PFA)/PBS at room temperature (for PCNT, P-ZAP70, and GzmB staining). Following fixation, the samples were washed in PBS for 5 min. PFA-fixed cells were permeabilized with 0.1% Triton and 1% BSA PBS. Following permeabilization, samples were washed in PBS for 5 min. Cells were stained with primary Abs ([1:30] CD3ζ; [1:50] P-ZAP70; [1:100] PTyr; [1:200] PCNT; [1:50] GzmB; see catalog number in the "Cells, plasmids, and Abs" section and Abs" section) overnight at 4°C. After washing with PBS, samples were incubated for 45 min at room temperature with Alexa Fluor 488– and 555–labeled secondary Abs and mounted with 90% glycerol/PBS.

Confocal microscopy was carried out on a Zeiss LSM700 (Carl Zeiss) microscope using a 63×/1.40 oil immersion objective. Images were acquired with pinholes opened to obtain 0.8 µm thick sections. Detectors were set to detect an optimal signal below the saturation limits. Images were processed with Zen 2009 image software (Carl Zeiss). Immunofluorescence analyses were carried out on medial optical sections of CD8⁺ T cell:APC conjugates using ImageJ (version 1.53a). Relative distances (µm) of the centrosome (marked by PCNT) from the center of the contact site with the APC and of the LGs (marked by GzmB) from the centrosome were measured using ImageJ (Fig. S2 A). Scoring of conjugates for the accumulation of CD3ζ or P-Tyr at the IS, or for centrosome (PCNT) juxtaposition to the IS membrane was based on the presence of the respective staining solely at the T cell–APC contact site and was expressed as a percentage of conjugates with synaptic staining versus the total number of conjugates analyzed. The recruitment index was calculated for each marker as the ratio of CD3ζ or p-Tyr fluorescence intensity at the synaptic area, which was manually defined at the T cell–APC contact site, to the remaining T cell area, using ImageJ.

Z-stacks were acquired on a spinning disk confocal and super-resolution microscope (CSU-W1-SoRA Nikon) with 60× oil objectives (numerical aperture 1.49) using a Photometrics BSI (Nikon). 3D Deconvolution (Richardson-Lucy method, 10 iterations) was applied to high-resolution imaging to improve the contrast of Video 2 and 3. 3D reconstructions were obtained using Fiji (version 2.1.0).

Flow cytometry and immunoblot

For flow cytometric analysis of protein tyrosine phosphorylation conjugates were formed as described in the “Conjugate formation, immunofluorescence microscopy, and analysis” section and incubated at 37°C for 1, 5, 15, and 30 min. Raji B cells were labeled as 1.5 µM CFSE (#C34554; Thermo Fisher Scientific) in PBS for 8 min at room temperature, then the staining reaction was stopped by adding BCS. CFSE-stained Raji B cells (0.1 × 10^6) were cocultured with CD8⁺ T cells (0.150 × 10^6), pretreated as described in “CTL pretreatments” section, for different time points. Conjugates were fixed for 15 min with 4% PFA/PBS, permeabilized with BD Perm/Wash Buffer (#51-2091KZ; BD Biosciences), stained with anti-PTyr Abs (clone 4G10, #05-32; Merk Millipore), and processed for flow cytometry, gating on CFSE negative ($CFSE^-$) cells.

1 × 10^6 purified CD8⁺ T cells (day 0) and CTLs (day 7) were used for immunoblot analysis of ACE2. For immunoblot analysis of Erk activation triggered by TCR crosslinking, CTLs (0.5 × 10^6 in 50 µl), pretreated with Spike W or PBS as described in the section “CTL pretreatments,” were activated for 0, 5, and 10 min at 37°C using anti-CD3ε (1 µg/ml, OKT3, #317302; BioLegend) and anti-CD28 (1 µg/ml, CD28.2, #302902; BioLegend) mAbs. Cells were pelleted, washed twice in ice-cold PBS, and lysed in

10–15 µl lysis buffer (0.5% Triton X-100 in 20 mM Tris-HCl, pH 8.0, 150 mM NaCl) in the presence of protease inhibitors (539,134; Calbiochem) and the phosphatase inhibitor sodium vanadate (S6508; Sigma-Aldrich). Lysates were cleared by centrifugation at 16,000 ×*g* for 20 min. Protein quantification in postnuclear supernatants was carried out using the BCA Assay kit (EMP014500; EuroClone). Proteins were resolved by SDS-PAGE and transferred to nitrocellulose membranes (#10600002; Amersham Protran). Immunoblotting was carried out using anti-phospho-Erk1/2 ([1:500], phosphorylated p44/42 [MAPK] Erk1/2, #9101; Cell Signaling), anti-Erk2 ([1:500], clone D2, #sc-1647; SantaCruz), anti-ACE2 ([1:500], clone SN0754, #MA5-32307; Invitrogen), and anti-actin ([1:10,000], #MAB1501; Merck Millipore) Abs and peroxidase-labeled secondary Ig, and a chemiluminescence detection kit (Pierce Rockford). Stripping was carried out by using Re-Blot Plus Mild Antibody Stripping Solution, 10× (#2502; Merck Millipore). Blots were scanned using a laser densitometer (Duoscan T2500; Agfa) and quantified using ImageJ 1.53a (National Institutes of Health).

RNA purification and RT-qPCR

RNA was extracted from CTLs (days 0, 5, and 7) using the RNeasy Plus Mini Kit (#74136; Qiagen), reverse transcribed to first-strand cDNAs using iScript cDNA Synthesis Kit (#1708891; Bio-Rad), and analyzed by RT-qPCR, as previously described (Onnis et al., 2015). Primer sequences for ACE2 amplified a region of 133 bp (forward: 5′-TCCATTGGTCTTCTGTCACCCGC-3′; reverse: 5′-AGACCATCCACCTCCACTTCTC-3′). Primer sequences for MAS1 amplified a region of 121 bp (forward: 5′-GCCCTGAGGAGACCGTAG-3′; reverse: 5′-ACAACAGCGGTT CTTGCTC-3′. Primer sequences for GrzmB amplified a region of 121 bp (forward: 5′-TCAAAGAACAGGAGCCGACC-3′; reverse: 5′-TTGGCCTTTCTCTCCAGCTG-3′). Primer sequences for 18S amplified a region of 64 bp: forward: 5′-CGCCGCTAG AGGTGAAATT-3′; reverse: 5′-CTTGGCAAATGCTTTCGC-3′. Differences in gene expression were calculated using the ΔΔCt method and normalized to 18S.

Degranulation and cytotoxicity assays

For the degranulation assay, Raji B cells were incubated with 1.5 µM CFSE (#C34554; Thermo Fisher Scientific) in PBS for 8 min at room temperature. Then the staining reaction was stopped by adding BCS. CFSE-stained Raji B cells (0.025×10^6) were loaded with 1 µg/ml Staphylococcal superantigens A, B, and E (+SAgs) for 1 h in serum-free AIM V medium, mixed with $CD8^+$ T cells (0.0625×10^6), pretreated as described above at an E:T ratio 2.5:1 in 50 µl AIMV medium containing APC-labeled anti-human CD107a (LAMP1) mAb (1:160) for 1 h at 37°C. Unpulsed CFSE-stained Raji B cells were used as the negative control (–SAgs). Cells were washed, resuspended in cold PBS, and acquired using a GUAVA flow cytometer (Merck Millipore). For immunofluorescence staining of surface LAMP1, cells were seeded onto poly-L-lysine–coated slides and fixed for 15 min in 4% PFA/PBS at room temperature. Following fixation, the samples were washed in PBS for 5 min. Cells were incubated for 45 min at room temperature with Alexa Fluor 555–labeled secondary Ab and mounted with 90% glycerol/PBS.

For the cytotoxicity assay, Raji B cells were stained with 500 nM of calcein-AM (#C1430; Invitrogen) in serum-free AIM V medium with 10 mM HEPES for 15 min at room temperature and then loaded with 2 µg/ml staphylococcal superantigens A, B, and E (+SAgs) for 2 h in serum-free AIM V medium (#12055-091; Gibco). SAg-pulsed Raji B cells used as target cells were settled in a 96-well black flat bottom plate (5×10^4 cells per well). Unpulsed CFSE-stained Raji B cells were used as negative control (–SAgs). CTLs (day 7) were added to target cells at different E:T ratios (i.e., 5:1, 10:1, 20:1 for analysis of cytotoxicity of CTLs (day 7; Fig. S1 C) and 2.5:1, 5:1, 10:1 for analysis of cytotoxicity of CTLs (day 7) pretreated with 0.05 µg/µl Spike W; Fig. 3 F) in 200 µl AIMV medium and incubated at 37°C up to 4 h to measure killing. Target cells alone and target cells lysed with 1% Triton X-100 were used as control samples. The decreased calcein fluorescence in target cells due to cell lysis was measured at 485 nm excitation wavelength and 528 nm emission wavelength in the bottom reading mode by using a Synergy HTX multimode plate reader (BioTek). Cytotoxicity (% target cell lysis) was calculated as follows: $(F_{live} - \gamma \times F_{exp})/(F_{live} - F_{lyse}) \times 100$, where F_{live} is the fluorescence of only target cell controls, F_{exp} is the CTLs with target cells, and F_{lyse} is the maximal target lysis in the presence of 1% Triton X-100. The γ value was measured at time zero using the formula $\gamma = F_{live}\ (0)/F_{exp}\ (0)$.

To analyze the effects of CTL pretreatments on cytotoxicity using a flow cytometry–based and antigen-specific assay, melanoma-specific CTLs, pretreated for 30 min at 20°C with either Spike W (1, 2.5, 5 µg/ml), 1.2×10^9/ml MiniVs, 2 µg/ml anti-ACE2 Ab, or PBS were cocultured with melanoma A375 cells in RPMI 10% FCS. The experiment was performed in duplicate at an E:T ratio of 5, 2.5, and 1. After 18 h, cells were collected and stained with FITC-labeled anti-CD8 mAb. Propidium iodide (#537059; Sigma-Aldrich) was added before each acquisition to measure the frequency of dead A375 cells. Flow cytometric analysis was carried out on BD FACS Canto II using the FACS-Diva software (Becton Dickinson).

ELISA

To measure IFNγ production, 2×10^5 CTLs specific for MAGE A3 melanoma antigen were seeded in duplicate in RPMI-1640 medium and cocultured with 10^5 irradiated autologous antigen-presenting cells and MAGE A3 antigen (2 µg/ml). CTLs of each melanoma patient were pretreated with PBS or Spike (1, 2.5, 5 µg/ml) or anti-ACE2 Ab for 30 min at 20°C. Alternatively, CTLs were cocultured with Spike-overexpressing A375 cells. Supernatant from each sample was collected after incubation for 36 h and then tested in duplicate for its content of IFNγ by ELISA (Invitrogen).

Statistics and reproducibility

Each experiment was performed at least three independent times. The exact number of repeats and the number of cells analyzed is specified in the figure legends. Statistical analyses were performed with Prism software (GraphPad Software). Pairwise or multiple comparisons of values with normal distribution were carried out with Student's *t* test (paired or unpaired), one-sample *t* test (theoretical mean = 1), and one-way

ANOVA test or one-sample *t* test (theoretical mean = 100), whereas values without Gaussian distribution were analyzed with Mann–Whitney test or Kruskal–Wallis test. Statistical significance was defined as: ****, $P \le 0.0001$; ***, $P \le 0.001$; **, $P \le 0.01$; *, $P \le 0.05$; n.s., not significant.

Online supplemental material

Included in the supplemental material are three supplementary figures showing the workflow for CTL generation, the parameters for IS image analysis, and the dose responses to Spike (Fig. S1); the outcome of Spike W pretreatment on IFNγ production by CTLs as well as the analysis of the effects of Spike W on IS signaling in freshly purified $CD8^+$ T cells (Fig. S2); and the quantification of the outcome of pretreatment with anti-ACE2 Ab on IFNγ production by CTLs, as well as the effects of anti-ACE2 Ab on the nascent and mature IS in CTLs (Fig. S3). Additionally, the supplemental material includes six videos. Videos 1, 2, and 3 show the 3D reconstruction of a representative CTL-APC conjugate formed with either SAg-unpulsed (Video 1) or SAg-pulsed (Videos 2 and 3) APCs and costained for PTyr and CD3ζ. CTLs used in SAg-specific conjugates were pretreated with either vehicle (Video 2) or Spike W (Video 3). Videos 4, 5, and 6 show the 3D reconstruction of representative CTL-APC conjugate formed with either SAg-unpulsed (Video 4) or SAg-pulsed (Videos 5 and 6) APCs and costained for PNCT and GzmB. CTLs used in SAg-specific conjugates were pretreated with either vehicle (Video 5) or Spike W (Video 6).

Acknowledgments

This article is dedicated to the memory of John L. Telford.

The authors wish to thank Hsin-Fang Chang (University of Saarland, Saarbrücken, Germany) for sharing the calcein release protocol, Mike Dustin (University of Oxford, Oxford, UK) for his support on the experiments with MiniVs, and Jason S. McLellan (University of Texas, Austin, TX) for generously providing the SARS-CoV-2 S-2P–encoding construct. The graphical abstract was created using BioRender.com.

This work was funded by European Research Council (ERC) Synergy Grant 951329 (ATTACK) and Associazione Italiana per la Ricerca sul Cancro grant IG-2017-20148 to C.T. Baldari, and ERC Advanced Grant 787552 to R. Rappuoli (vAMRes). O. Staufer was funded by an ERC Marie Sklodowska Curie Actions/UK Engineering and Physical Science Research Council fellowship (E. Pantano/X023907/1). This work was supported by a fundraising activity promoted by Unicoop Firenze, Coop Alleanza 3.0, Unicoop Tirreno, Coop Centro Italia, Coop Reno, and Coop Amiatina.

Author contributions: A. Onnis, E. Andreano, C. Cassioli, F. Finetti, and C. Della Bella performed the experiments; A. Onnis, C. Cassioli, F. Finetti, and C. Della Bella analyzed the data and prepared the figures; A. Onnis, E. Andreano, M.M. D'Elios, R. Rappuoli, and C.T. Baldari wrote the paper; O. Staufer, E. Pantano, V. Abbiento, and G. Marotta provided essential reagents.

Disclosures: E. Andreano reported patent number 102020000015754 issued, patent number 102020000018955 issued, patent number 102020000029969 issued, and apatent to PCT/IB2021/055755 issued. E. Pantano reported a patent to 102020000015754 issued, a patent to 102020000018955 issued, a patent to 102020000029969 issued, and a patent to PCT/IB2021/055755 issued. V. Abbiento reported patent number 102020000015754 issued, patent number 102020000018955 issued, patent number 102020000029969 issued, and a patent to PCT/IB2021/055755 issued. No other disclosures were reported.

Submitted: 23 May 2022
Revised: 28 June 2022
Accepted: 2 November 2022

References

Amedei, A., C. Della Bella, E. Niccolai, N. Stanflin, M. Benagiano, R. Duranti, G. Del Prete, T.F. Murphy, and M.M. D'Elios. 2009. Moraxella catarrhalis-specific Th1 cells in BAL fluids of chronic obstructive pulmonary disease patients. *Int. J. Immunopathol. Pharmacol.* 22:979–990. https://doi.org/10.1177/039463200902200413

Andreano, E., E. Nicastri, I. Paciello, P. Pileri, N. Manganaro, G. Piccini, A. Manenti, E. Pantano, A. Kabanova, M. Troisi, et al. 2021a. Extremely potent human monoclonal antibodies from COVID-19 convalescent patients. *Cell*. 184:1821–1835.e16. https://doi.org/10.1016/j.cell.2021.02.035

Andreano, E., I. Paciello, G. Piccini, N. Manganaro, P. Pileri, I. Hyseni, M. Leonardi, E. Pantano, V. Abbiento, L. Benincasa, et al. 2021b. Hybrid immunity improves B cells and antibodies against SARS-CoV-2 variants. *Nature*. 600:530–535. https://doi.org/10.1038/s41586-021-04117-7

Au-Yeung, B.B., N.H. Shah, L. Shen, and A. Weiss. 2018. ZAP-70 in signaling, Biology, and disease. *Annu. Rev. Immunol.* 36:127–156. https://doi.org/10.1146/annurev-immunol-042617-053335

Bastard, P., L.B. Rosen, Q. Zhang, E. Michailidis, H.H. Hoffmann, Y. Zhang, K. Dorgham, Q. Philippot, J. Rosain, V. Béziat, et al. 2020. Autoantibodies against type I IFNs in patients with life-threatening COVID-19. *Science*. 370:eabd485. https://doi.org/10.1126/science.abd4585

Bar-On, Y.M., A. Flamholz, R. Phillips, and R. Milo. 2020. SARS-CoV-2 (COVID-19) by the numbers. *Elife*. 9:e57309. https://doi.org/10.7554/eLife.57309

Batista, F.D., D. Iber, and M.S. Neuberger. 2001. B cells acquire antigen from target cells after synapse formation. *Nature*. 411:489–494. https://doi.org/10.1038/35078099

Blumenthal, D., and J.K. Burkhardt. 2020. Multiple actin networks coordinate mechanotransduction at the immunological synapse. *J. Cell Biol.* 219:e201911058. https://doi.org/10.1083/jcb.201911058

Camargo, S.M., D. Singer, V. Makrides, K. Huggel, K.M. Pos, C.A. Wagner, K. Kuba, U. Danilczyk, F. Skovby, R. Kleta, et al. 2009. Tissue-specific amino acid transporter partners ACE2 and collectrin differentially interact with hartnup mutations. *Gastroenterology*. 136:872–882. https://doi.org/10.1053/j.gastro.2008.10.055

Cassioli, C., and C.T. Baldari. 2022. The expanding arsenal of cytotoxic T cells. *Front. Immunol.* 13:883010. https://doi.org/10.3389/fimmu.2022.883010

Cassioli, C., S. Balint, E.B. Compeer, J.H. Felce, A. Gamberucci, C. Della Bella, S.L. Felce, J. Brunetti, S. Valvo, D. Pende, et al. 2021a. Increasing LFA-1 expression Enhances immune synapse architecture and T cell receptor signaling in Jurkat E6.1 cells. *Front. Cell Dev. Biol.* 9:673446. https://doi.org/10.3389/fcell.2021.673446

Cassioli, C., A. Onnis, F. Finetti, N. Capitani, J. Brunetti, E.B. Compeer, V. Niederlova, O. Stepanek, M.L. Dustin, and C.T. Baldari. 2021b. The Bardet-Biedl syndrome complex component BBS1 controls T cell polarity during immune synapse assembly. *J. Cell Sci.* 134:jcs258462. https://doi.org/10.1242/jcs.258462

Chaouat, A.E., I. Brizic, P. Kucan Brlic, N. Atari, L. Kliker, O. Alfi, M. Mandelboim, D. Wolf, L. Tafish, I. Kol, et al. 2022. Anti-human ACE2 antibody neutralizes and inhibits virus production of SARS-CoV-2 variants of concern. *iScience*. 25:104935. https://doi.org/10.1016/j.isci.2022.104935

Chemin, K., A. Bohineust, S. Dogniaux, M. Tourret, S. Guégan, F. Miro, and C. Hivroz. 2012. Cytokine secretion by $CD4^+$ T cells at the immunological synapse requires Cdc42-dependent local actin remodeling but not microtubule organizing center polarity. *J. Immunol.* 189:2159–2168. https://doi.org/10.4049/jimmunol.1200156

Chen, Y., Y.N. Zhang, R. Yan, G. Wang, Y. Zhang, Z.R. Zhang, Y. Li, J. Ou, W. Chu, Z. Liang, et al. 2021. ACE2-targeting monoclonal antibody as potent and broad-spectrum coronavirus blocker. *Signal Transduct. Targeted Ther.* 6:315. https://doi.org/10.1038/s41392-021-00740-y

Chen, Z., and E. John Wherry. 2020. T cell responses in patients with COVID-19. *Nat. Rev. Immunol.* 20:529–536. https://doi.org/10.1038/s41577-020-0402-6

Chua, R.L., S. Lukassen, S. Trump, B.P. Hennig, D. Wendisch, F. Pott, O. Debnath, L. Thürmann, F. Kurth, M.T. Völker, et al. 2020. COVID-19 severity correlates with airway epithelium-immune cell interactions identified by single-cell analysis. *Nat. Biotechnol.* 38:970–979. https://doi.org/10.1038/s41587-020-0602-4

Clarke, N.E., M.J. Fisher, K.E. Porter, D.W. Lambert, and A.J. Turner. 2012. Angiotensin converting enzyme (ACE) and ACE2 bind integrins and ACE2 regulates integrin signalling. *PLoS One.* 7:e34747. https://doi.org/10.1371/journal.pone.0034747

Coppo, M., M. Bandinelli, A. Berni, S. Galastri, R. Abbate, L. Poggesi, F. Marra, G.F. Gensini, and M. Boddi. 2011. Ang II Upregulation of the T-lymphocyte renin-angiotensin system is amplified by low-grade inflammation in human hypertension. *Am. J. Hypertens.* 24:716–723. https://doi.org/10.1038/ajh.2011.32

D'Elios, M.M., R. Josien, M. Manghetti, A. Amedei, M. de Carli, M.C. Cuturi, G. Blancho, F. Buzelin, G. del Prete, and J.P. Soulillou. 1997. Predominant Th1 cell infiltration in acute rejection episodes of human kidney grafts. *Kidney Int.* 51:1876–1884. https://doi.org/10.1038/ki.1997.256

Daniele, T., Y. Hackmann, A.T. Ritter, M. Wenham, S. Booth, G. Bossi, M. Schintler, M. Auer-Grumbach, and G.M. Griffiths. 2011. A role for Rab7 in the movement of secretory granules in cytotoxic T lymphocytes. *Traffic.* 12:902–911. https://doi.org/10.1111/j.1600-0854.2011.01194.x

Danilczyk, U., R. Sarao, C. Remy, C. Benabbas, G. Stange, A. Richter, S. Arya, J.A. Pospisilik, D. Singer, S.M. Camargo, et al. 2006. Essential role for collectrin in renal amino acid transport. *Nature.* 444:1088–1091. https://doi.org/10.1038/nature05475

Douanne, T., and G.M. Griffiths. 2021. Cytoskeletal control of the secretory immune synapse. *Curr. Opin. Cell Biol.* 71:87–94. https://doi.org/10.1016/j.ceb.2021.02.008

Dustin, M.L., and K. Choudhuri. 2016. Signaling and polarized communication across the T cell immunological synapse. *Annu. Rev. Cell Dev. Biol.* 32:303–325. https://doi.org/10.1146/annurev-cellbio-100814-125330

Fackler, O.T., A. Alcover, and O. Schwartz. 2007. Modulation of the immunological synapse: A key to HIV-1 pathogenesis? *Nat. Rev. Immunol.* 7:310–317. https://doi.org/10.1038/nri2041

Hoffmann, M., H. Kleine-Weber, S. Schroeder, N. Krüger, T. Herrler, S. Erichsen, T.S. Schiergens, G. Herrler, N.H. Wu, A. Nitsche, et al. 2020. SARS-CoV-2 cell entry depends on ACE2 and TMPRSS2 and is blocked by a clinically proven protease inhibitor. *Cell.* 181:271–280.e8. https://doi.org/10.1016/j.cell.2020.02.052

Inoue, Y., N. Tanaka, Y. Tanaka, S. Inoue, K. Morita, M. Zhuang, T. Hattori, and K. Sugamura. 2007. Clathrin-dependent entry of severe acute respiratory syndrome coronavirus into target cells expressing ACE2 with the cytoplasmic tail deleted. *J. Virol.* 81:8722–8729. https://doi.org/10.1128/JVI.00253-07

Irvine, D.J., M.A. Purbhoo, M. Krogsgaard, and M.M. Davis. 2002. Direct observation of ligand recognition by T cells. *Nature.* 419:845–849. https://doi.org/10.1038/nature01076

Kabanova, A., F. Sanseviero, V. Candi, A. Gamberucci, A. Gozzetti, G. Campoccia, M. Bocchia, and C.T. Baldari. 2016. Human cytotoxic T lymphocytes form dysfunctional immune synapses with B cells characterized by non-polarized lytic granule release. *Cell Rep.* 15:9–18. https://doi.org/10.1016/j.celrep.2016.02.084

Kalfaoglu, B., J. Almeida-Santos, C.A. Tye, Y. Satou, and M. Ono. 2021. T-cell dysregulation in COVID-19. *Biochem. Biophys. Res. Commun.* 538:204–210. https://doi.org/10.1016/j.bbrc.2020.10.079

Kowalczuk, S., A. Bröer, N. Tietze, J.M. Vanslambrouck, J.E. Rasko, and S. Bröer. 2008. A protein complex in the brush-border membrane explains a Hartnup disorder allele. *FASEB J.* 22:2880–2887. https://doi.org/10.1096/fj.08-107300

Kummerow, C., E.C. Schwarz, B. Bufe, F. Zufall, M. Hoth, and B. Qu. 2014. A simple, economic, time-resolved killing assay. *Eur. J. Immunol.* 44:1870–1872. https://doi.org/10.1002/eji.201444518

Lambert, D.W., N.E. Clarke, N.M. Hooper, and A.J. Turner. 2008. Calmodulin interacts with angiotensin-converting enzyme-2 (ACE2) and inhibits shedding of its ectodomain. *FEBS Lett.* 582:385–390. https://doi.org/10.1016/j.febslet.2007.11.085

Liao, M., Y. Liu, J. Yuan, Y. Wen, G. Xu, J. Zhao, L. Cheng, J. Li, X. Wang, F. Wang, et al. 2020. Single-cell landscape of bronchoalveolar immune cells in patients with COVID-19. *Nat. Med.* 26:842–844. https://doi.org/10.1038/s41591-020-0901-9

Lin, Q., R.S. Keller, B. Weaver, and L.S. Zisman. 2004. Interaction of ACE2 and integrin beta1 in failing human heart. *Biochim. Biophys. Acta.* 1689:175–178. https://doi.org/10.1016/j.bbadis.2004.05.005

Martín-Cófreces, N.B., and F. Sánchez-Madrid. 2018. Sailing to and docking at the immune synapse: Role of tubulin dynamics and molecular motors. *Front. Immunol.* 9:1174. https://doi.org/10.3389/fimmu.2018.01174

Mentlik, A.N., K.B. Sanborn, E.L. Holzbaur, and J.S. Orange. 2010. Rapid lytic granule convergence to the MTOC in natural killer cells is dependent on dynein but not cytolytic commitment. *Mol. Biol. Cell.* 21:2241–2256. https://doi.org/10.1091/mbc.e09-11-0930

Norris, E.G., X.S. Pan, and D.C. Hocking. 2022. Receptor binding domain of SARS-CoV-2 is a functional αv-integrin agonist. *bioRxiv*. https://doi.org/10.1101/2022.04.11.487882 (Preprint posted April 11, 2022)

Onnis, A., F. Finetti, L. Patrussi, M. Gottardo, C. Cassioli, S. Spanò, and C.T. Baldari. 2015. The small GTPase Rab29 is a common regulator of immune synapse assembly and ciliogenesis. *Cell Death Differ.* 22:1687–1699. https://doi.org/10.1038/cdd.2015.17

Papa, I., and C.G. Vinuesa. 2018. Synaptic interactions in germinal centers. *Front. Immunol.* 9:1858. https://doi.org/10.3389/fimmu.2018.01858

Park, E.J., P.K. Myint, M.G. Appiah, S. Darkwah, S. Caidengbate, A. Ito, E. Matsuo, E. Kawamoto, A. Gaowa, and M. Shimaoka. 2021. The spike glycoprotein of SARS-CoV-2 binds to β1 integrins expressed on the surface of lung epithelial cells. *Viruses.* 13:645. https://doi.org/10.3390/v13040645

Samavati, L., and B.D. Uhal. 2020. ACE2, much more than Just a receptor for SARS-COV-2. *Front. Cell. Infect. Microbiol.* 10:317. https://doi.org/10.3389/fcimb.2020.00317

Sender, R., Y.M. Bar-On, S. Gleizer, B. Bernshtein, A. Flamholz, R. Phillips, and R. Milo. 2021. The total number and mass of SARS-CoV-2 virions. *Proc. Natl. Acad. Sci. USA.* 118:e2024815118. https://doi.org/10.1073/pnas.2024815118

Sigrist, C.J., E. de Castro, L. Cerutti, B.A. Cuche, N. Hulo, A. Bridge, L. Bougueleret, and I. Xenarios. 2013. New and continuing developments at PROSITE. *Nucleic Acids Res.* 41:D344–D347. https://doi.org/10.1093/nar/gks1067

Silva-Filho, J.L., C. Caruso-Neves, and A.A. Pinheiro. 2016. Angiotensin II type-1 receptor (AT_1R) regulates expansion, differentiation, and functional capacity of antigen-specific $CD8^+$ T cells. *Sci. Rep.* 6:35997. https://doi.org/10.1038/srep35997

Silva-Filho, J.L., C. Caruso-Neves, and A.A. Pinheiro. 2017. Targeting angiotensin II type-1 receptor (AT_1R) inhibits the harmful phenotype of plasmodium-specific $CD8^+$ T cells during blood-stage malaria. *Front. Cell. Infect. Microbiol.* 7:42. https://doi.org/10.3389/fcimb.2017.00042

Simons, P., D.A. Rinaldi, V. Bondu, A.M. Kell, S. Bradfute, D.S. Lidke, and T. Buranda. 2021. Integrin activation is an essential component of SARS-CoV-2 infection. *Sci. Rep.* 11:20398. https://doi.org/10.1038/s41598-021-99893-7

Springer, T.A., and M.L. Dustin. 2012. Integrin inside-out signaling and the immunological synapse. *Curr. Opin. Cell Biol.* 24:107–115. https://doi.org/10.1016/j.ceb.2011.10.004

Staufer, O., K. Gupta, J.E. Hernandez Bücher, F. Kohler, C. Sigl, G. Singh, K. Vasileiou, A. Yagüe Relimpio, M. Macher, S. Fabritz, et al. 2022. Synthetic virions reveal fatty acid-coupled adaptive immunogenicity of SARS-CoV-2 spike glycoprotein. *Nat. Commun.* 13:868. https://doi.org/10.1038/s41467-022-28446-x

Torres, J.L., G. Ozorowski, E. Andreano, H. Liu, J. Copps, G. Piccini, L. Donnici, M. Conti, C. Planchais, D. Planas, et al. 2022. Structural insights of a highly potent pan-neutralizing SARS-CoV-2 human monoclonal antibody. *Proc. Natl. Acad. Sci. USA.* 119:e2120976119. https://doi.org/10.1073/pnas.2120976119

Welch, J.L., J. Xiang, Q. Chang, J.C.D. Houtman, and J.T. Stapleton. 2022. T-cell expression of angiotensin-converting enzyme 2 and binding of severe acute respiratory coronavirus 2. *J. Infect. Dis.* 225:810–819. https://doi.org/10.1093/infdis/jiab595

Wen, W., W. Su, H. Tang, W. Le, X. Zhang, Y. Zheng, X. Liu, L. Xie, J. Li, J. Ye, et al. 2020. Immune cell profiling of COVID-19 patients in the recovery stage by single-cell sequencing. *Cell Discov.* 6:31. https://doi.org/10.1038/s41421-020-0168-9

Wrapp, D., N. Wang, K.S. Corbett, J.A. Goldsmith, C.L. Hsieh, O. Abiona, B.S. Graham, and J.S. McLellan. 2020. Cryo-EM structure of the 2019-nCoV spike in the prefusion conformation. *Science.* 367:1260–1263. https://doi.org/10.1126/science.abb2507

Yin, W., Y. Xu, P. Xu, X. Cao, C. Wu, C. Gu, X. He, X. Wang, S. Huang, Q. Yuan, et al. 2022. Structures of the Omicron spike trimer with ACE2 and an anti-Omicron antibody. *Science*. 375:1048–1053. https://doi.org/10.1126/science.abn8863

Zhang, H., J. Wada, K. Hida, Y. Tsuchiyama, K. Hiragushi, K. Shikata, H. Wang, S. Lin, Y.S. Kanwar, and H. Makino. 2001. Collectrin, a collecting duct-specific transmembrane glycoprotein, is a novel homolog of ACE2 and is developmentally regulated in embryonic kidneys. *J. Biol. Chem.* 276:17132–17139. https://doi.org/10.1074/jbc.M006723200

Zhang, J.D., M.B. Patel, Y.S. Song, R. Griffiths, J. Burchette, P. Ruiz, M.A. Sparks, M. Yan, D.N. Howell, J.A. Gomez, et al. 2012. A novel role for type 1 angiotensin receptors on T lymphocytes to limit target organ damage in hypertension. *Circ. Res.* 110:1604–1617. https://doi.org/10.1161/CIRCRESAHA.111.261768

Zhang, Q., P. Bastard, Z. Liu, J. Le Pen, M. Moncada-Velez, J. Chen, M. Ogishi, I.K.D. Sabli, S. Hodeib, C. Korol, et al. 2020. Inborn errors of type I IFN immunity in patients with life-threatening COVID-19. *Science*. 370: eabd4570. https://doi.org/10.1126/science.abd4570

Zheng, M., Y. Gao, G. Wang, G. Song, S. Liu, D. Sun, Y. Xu, and Z. Tian. 2020. Functional exhaustion of antiviral lymphocytes in COVID-19 patients. *Cell Mol. Immunol.* 17:533–535. https://doi.org/10.1038/s41423-020-0402-2

Supplemental material

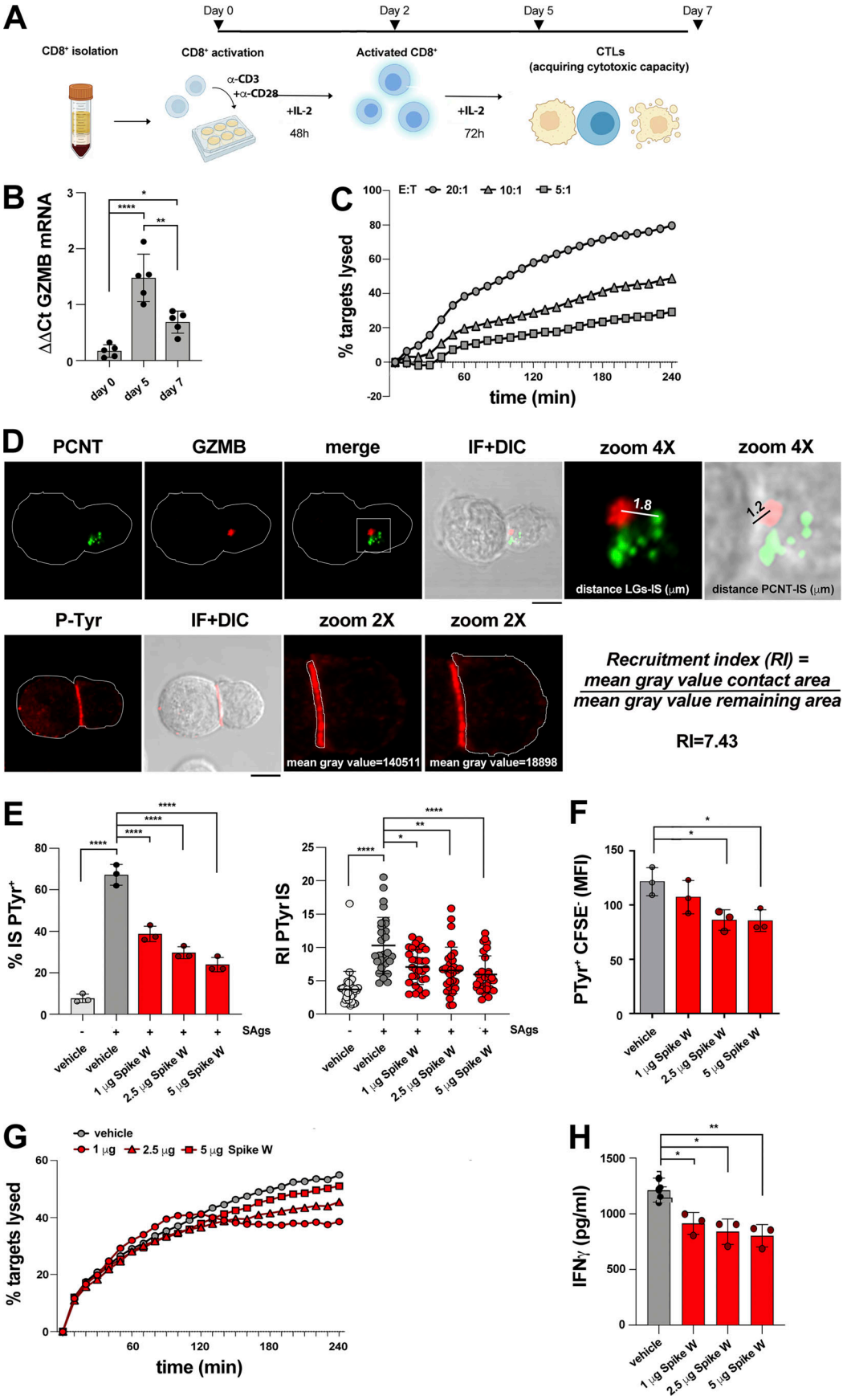
A
Day 0
Day 2
Day 5
Day 7
CD8+ isolation
CD8+ activation
Activated CD8+
CTLs
(acquiring cytotoxic capacity)
α-CD3
+α-CD28
+IL-2
48h
+IL-2
72h
B
ΔΔCt GZMB mRNA
day 0
day 5
day 7
C
E:T 20:1 10:1 5:1
% targets lysed
time (min)
D
PCNT
GZMB
merge
IF+DIC
zoom 4X
zoom 4X
1.8
1.2
distance LGs-IS (μm)
distance PCNT-IS (μm)
P-Tyr
IF+DIC
zoom 2X
zoom 2X
mean gray value=140511
mean gray value=18898
Recruitment index (RI) =
mean gray value contact area
mean gray value remaining area
RI=7.43
E
% IS PTyr+
RI PTyr IS
SAgs
vehicle
vehicle
1 μg Spike W
2.5 μg Spike W
5 μg Spike W
F
PTyr+ CFSE- (MFI)
G
vehicle
1 μg
2.5 μg
5 μg Spike W
% targets lysed
time (min)
H
IFNγ (pg/ml)

Figure S1. **Experimental settings used. (A)** Workflow for CTL generation from CD8⁺ T cells purified from buffy coats of healthy donors. **(B)** RT-qPCR of human GzmB mRNA in purified CD8⁺ T cells at days 0, 5, and 7 after stimulation with anti-CD3/CD28 mAb–coated beads in the presence of IL-2 (n = 5, one-way ANOVA test; ****, P ≤ 0.0001; **, P ≤ 0.01; *, P ≤ 0.05). **(C)** Fluorimetric analysis of cytotoxicity of CTLs (day 7) generated as depicted in A, using the real-time calcein release–based killing assay. The killing process was monitored in different CTL:target cell ratios over time by measuring the release of calcein fluorescence every 10 min for 4 h. Representative curves showing the kinetics of target cell lysis by CTLs at the indicated CTL:target cell ratios are shown (n = 3). **(D)** Top: Image of a representative CD8⁺ T cell (day 7) conjugated with SAg-pulsed Raji B cells for 15 min and co-stained with anti-PCNT and anti-GzmB Abs. The CD8⁺ T cell was magnified to depict the parameters used for quantification in Figs. 3, 4, and 5; and Figs. S2 and S3. A line from the center of each LG (marked by GzmB) to the center of the centrosome (marked by PCNT) was drawn to measure the distance (µm) between LGs and centrosome. A line from the center of the centrosome (marked by PCNT) of the CD8⁺ T cell to the center of the contact area with the Raji cell was drawn to measure the distance (µm) between the centrosome and the T cell:APC contact area. Bottom: Image of a representative CD8⁺ T cell (day 7) conjugated with SAg-pulsed Raji B cells for 15 min and stained with anti-PTyr mAb. The T cell was magnified to depict the parameters used for quantification in Figs. 1, 2, 4, and 5; and Figs. S2 and S3. Masks around both the contact area of CD8⁺ T cell:APC and in the remaining CD8⁺ T cell area were drawn to measure the mean gray value. The recruitment index (RI) was calculated as specified. **(E)** Immunofluorescence analysis of PTyr in CTLs (day 7) pretreated with either vehicle (PBS) or different concentrations of Spike W, then mixed with Raji cells (APCs) either unpulsed or pulsed with a combination of SEA, SEB, and SEE (SAgs), and incubated for 15 min at 37°C. Left: Quantification (%) of conjugates harboring PTyr staining at the IS (100 cells/sample, n = 3, one-way ANOVA test; ****, P ≤ 0.0001). Right: Relative PTyr fluorescence intensity at the IS (10 cells/sample, n = 3, Kruskal–Wallis test; ****, P ≤ 0.0001; **, P ≤ 0.01; *, P ≤ 0.05). **(F)** Flow cytometric analysis of conjugates prepared as in E. Raji cells were loaded with 5 µM CFSE prior to conjugate formation. Conjugates were stained anti-PTyr mAb followed by fluorescently labeled secondary Abs. The analysis was carried out gating on CSFE⁻ cells (n = 3, one-way ANOVA test; *, P ≤ 0.05). **(G)** Fluorimetric analysis of cytotoxicity of CTLs (day 7) using the calcein release assay. CTLs were pretreated with either vehicle (PBS) or different concentrations of Spike W and co-cultured with SAg-pulsed, calcein AM–loaded Raji cells at a E:T cell ratio 10:1 for 4 h. The representative curves show the kinetics of target cell lysis by CTLs at the different concentrations of Spike W (n = 3). **(H)** ELISA-based quantification of IFNγ in 36-h supernatants of melanoma-specific CTLs, pretreated with either vehicle (PBS) or different concentrations of Spike W and co-cultured with irradiated autologous APCs pulsed with 2 µg/ml MAGE 3 (n = 3, one-way ANOVA test; **, P ≤ 0.01; *, P ≤ 0.05). Data are expressed as mean ± SD. Nonsignificant differences are not shown. Scale bar, 5 µm.

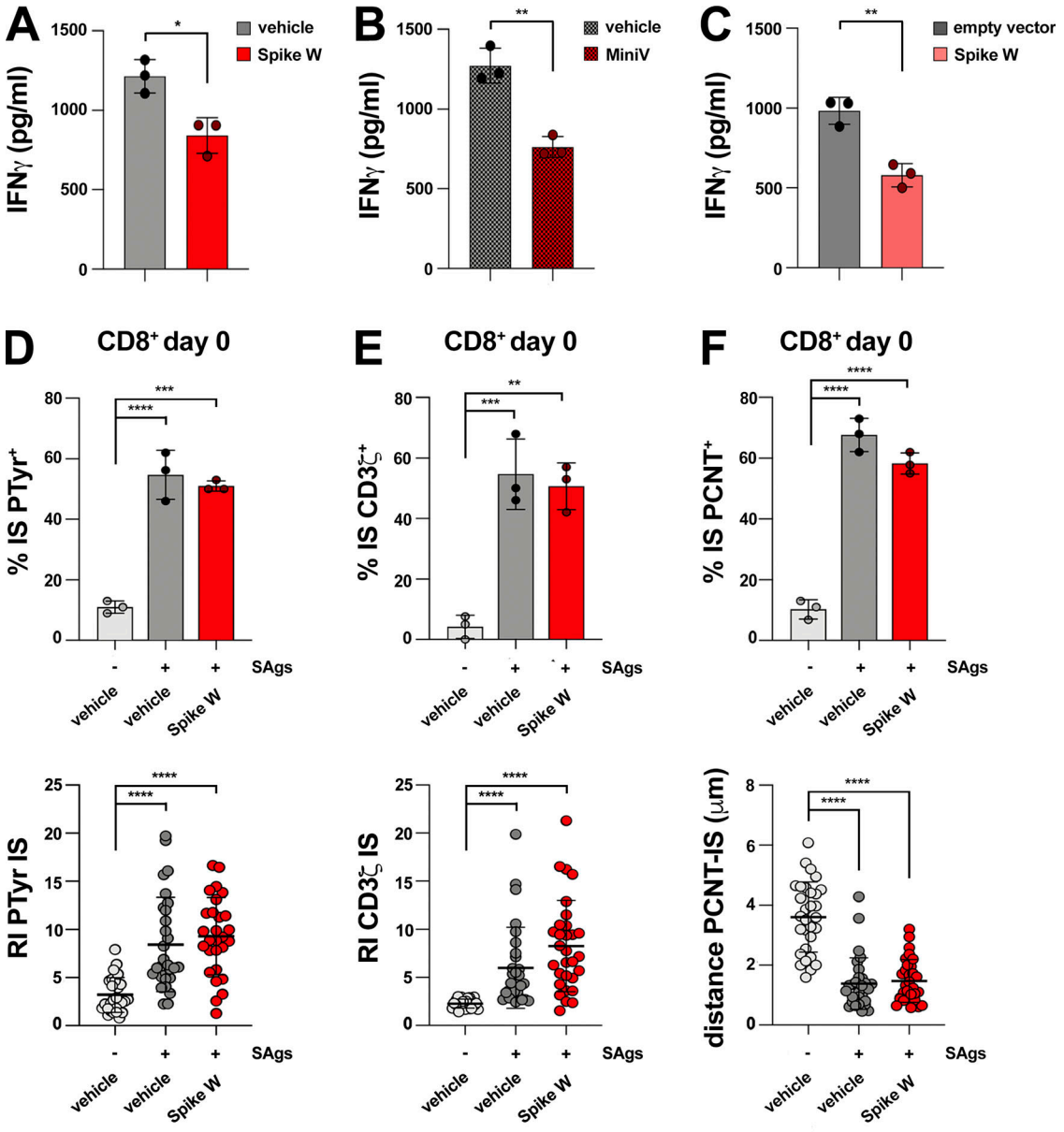

Figure S2. **Spike suppresses IS assembly and function in CTLs but not in resting CD8⁺ T cells. (A and B)** ELISA-based quantification of IFNγ in 36-h supernatants of melanoma-specific CTLs derived from three patients, pretreated with either vehicle (PBS) or Spike W (A), or with 1.2 × 10^9 liposomes or MiniVs (B), and co-cultured with irradiated autologous APCs pulsed with 2 µg/ml MAGE 3 (n = 3, unpaired two-tailed Student's t test; **, P ≤ 0.01; *, P ≤ 0.05). **(C)** ELISA-based quantification of IFNγ in 36-h supernatants of melanoma-specific CTLs derived from three patients, co-cultured with A375 melanoma cells transiently transfected with either a construct encoding Spike W or the empty control vector (n = 3, unpaired two-tailed Student's t test; **, P ≤ 0.01). **(D–F)** Top: Immunofluorescence analysis of PTyr in freshly purified CD8⁺ T cells (day 0) pretreated with either vehicle (PBS) or 0.05 µg/µl Spike W, then mixed with Raji cells (APCs) either unpulsed or pulsed with a combination of SEA, SEB, and SEE (SAgs), and incubated for 15 min at 37°C. The histograms show the quantification (%) of conjugates harboring PTyr (D), CD3ζ (E), or PCNT (F) staining at the IS (≥50 cells/sample, n = 3, one-way ANOVA test; ****, P ≤ 0.0001; ***, P ≤ 0.001; **, P ≤ 0.01). Bottom: Relative PTyr (D) and CD3ζ (E) fluorescence intensity at the IS (recruitment index; 10 cells/sample, n = 3, Kruskal–Wallis test; ****, P ≤ 0.0001). Measurement of the distance (µm) of the centrosome (PCNT) from the T cell–APC contact site (F; 10 cells/sample, n = 3, Kruskal–Wallis test; ****, P ≤ 0.0001). The data are expressed as mean ± SD.

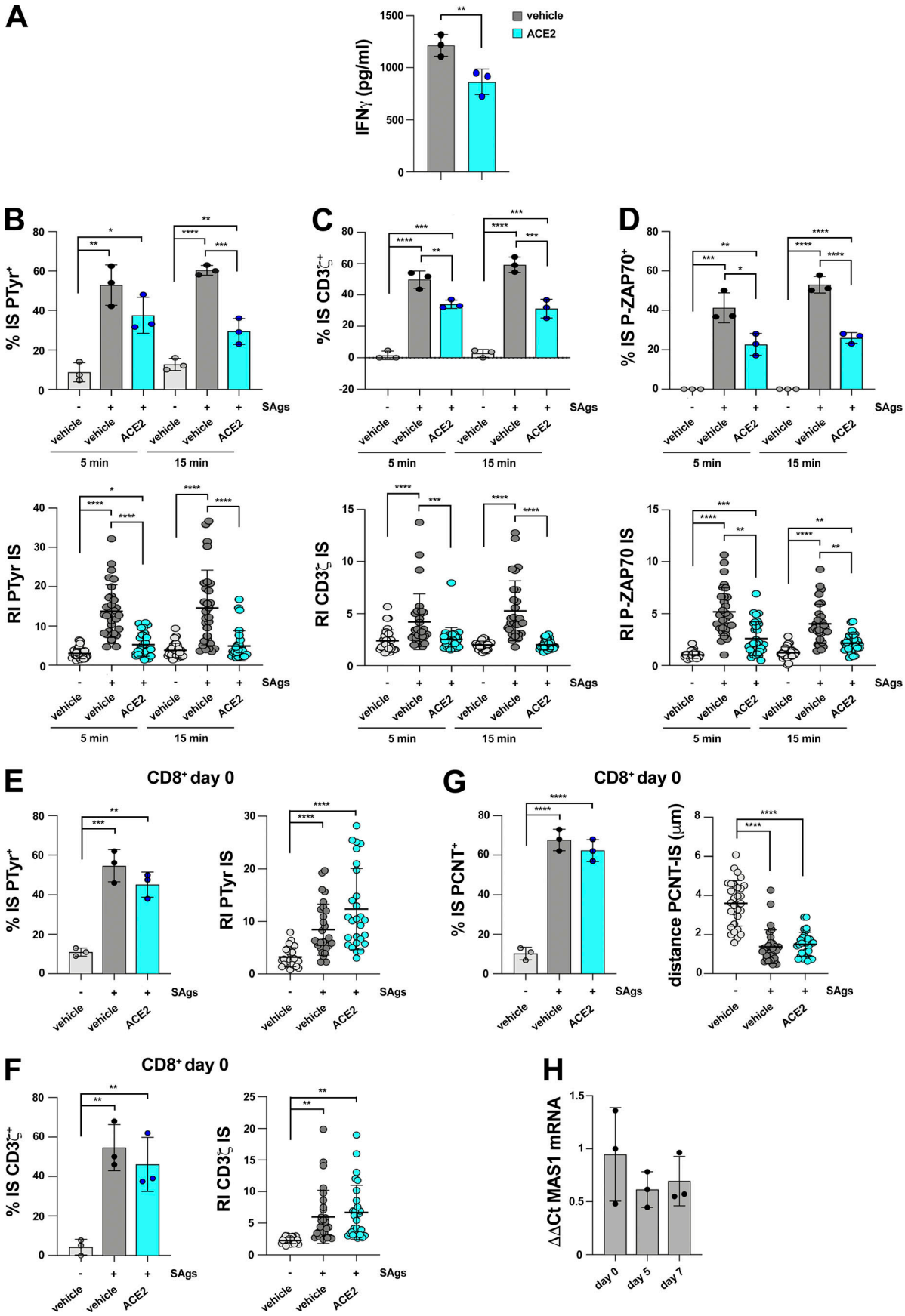
A
IFNγ (pg/ml)
vehicle
ACE2
B
% IS PTyr+
RI PTyr IS
C
% IS CD3ζ+
RI CD3ζ IS
D
% IS P-ZAP70+
RI P-ZAP70 IS
SAgs
vehicle
ACE2
5 min
15 min
E
CD8+ day 0
% IS PTyr+
RI PTyr IS
F
CD8+ day 0
% IS CD3ζ+
RI CD3ζ IS
G
CD8+ day 0
% IS PCNT+
distance PCNT-IS (μm)
H
ΔΔCt MAS1 mRNA
day 0
day 5
day 7

Figure S3. **ACE2 suppresses IS assembly and function in CTLs but not in resting CD8⁺ T cells. (A)** ELISA-based quantification of IFNγ in 36-h supernatants of melanoma-specific CTLs derived from three patients, pretreated with either vehicle (PBS) or 2 µg/ml anti-ACE2 Ab (ACE2), and co-cultured with irradiated autologous APCs pulsed with 2 µg/ml MAGE 3 (n = 3, unpaired two-tailed Student's t test; **, P ≤ 0.01). **(B–D)** Top: Quantification (%) of 5-min and 15-min conjugates harboring PTyr (B), CD3ζ (C), or P-ZAP-70 (D) staining at the IS (≥50 cells/sample, n = 3, one-way ANOVA test; ****, P ≤ 0.0001; ***, P ≤ 0.001; **, P ≤ 0.01; *, P ≤ 0.05). CTLs (day 7), pretreated with vehicle (PBS) or 2 µg/ml anti-ACE2 Ab (ACE2), were conjugated with Raji cells (APCs) in the absence or presence of SAgs and either an anti-ACE2 Ab, or Ang II, or the peptide Ang 1-7 (≥50 cells/sample, n = 3, one-way ANOVA test). Bottom: Relative PTyr (B), CD3ζ (C), or ZAP-70 (D) fluorescence intensity at the IS (recruitment index; 10 cells/sample, n = 3, Kruskal–Wallis test; ****, P ≤ 0.0001; ***, P ≤ 0.001; **, P ≤ 0.01; *, P ≤ 0.05). **(E and F)** Immunofluorescence analysis of PTyr and CD3ζ in freshly purified CD8⁺ T cells (day 0) pretreated with either vehicle (PBS) or 2 µg/ml anti-ACE2 Ab (ACE2), then mixed with Raji cells (APCs) either unpulsed or pulsed with a combination of SEA, SEB, and SEE (SAgs), and incubated for 15 min at 37°C. Left: Quantification (%) of conjugates harboring PTyr (E), CD3ζ (F; ≥50 cells/sample, n = 3, one-way ANOVA test; ***, P ≤ 0.001; **, P ≤ 0.01). Right: Relative PTyr (E) and CD3ζ (F) fluorescence intensity at the IS (recruitment index; 10 cells/sample, n = 3, Kruskal–Wallis test; ****, P ≤ 0.0001; **, P ≤ 0.01). **(G)** Immunofluorescence analysis of PCNT in conjugates formed as described in E and F. Left: Quantification (%) of conjugates harboring PCNT at the IS (≥50 cells/sample, n = 3, one-way ANOVA test; ****, P ≤ 0.0001). Right: Measurement of the distance (µm) of the centrosome (PCNT) from the T cell–APC contact site (10 cells/sample, n = 3, Kruskal–Wallis test; ****, P ≤ 0.0001). **(H)** RT-qPCR of human MAS1 mRNA in purified CD8⁺ T cells at days 0, 5, and 7 after stimulation with anti-CD3/CD28 mAb-coated beads in the presence of IL-2 (n = 3). Nonsignificant differences are not shown.

Video 1. **3D reconstruction of a representative CTL-APC conjugate formed with SAg-unpulsed APCs.** CTLs were pre-treated with vehicle and used to form conjugates with unpulsed Raji cells. Conjugates were co-stained for PTyr (orange) and CD3ζ (green). The playback frame rate is 7 frames/s.

Video 2. **3D reconstruction of a representative CTL-APC conjugate formed with SAg-pulsed APCs.** CTLs were pre-treated with vehicle and used to form conjugates with SAg-pulsed Raji cells. Conjugates were co-stained for PTyr (orange) and CD3ζ (green). The playback frame rate is 7 frames/s.

Video 3. **3D reconstruction of a representative CTL-APC conjugate formed with SAg-pulsed APCs.** CTLs were pre-treated with Spike W and used to form conjugates with SAg-pulsed Raji cells. Conjugates were co-stained for PTyr (orange) and CD3ζ (green). The playback frame rate is 7 frames/s.

Video 4. **3D reconstruction of a representative CTL-APC conjugate formed with SAg-unpulsed APCs.** CTLs were pre-treated with vehicle and used to form conjugates with unpulsed Raji cells. Conjugates were co-stained for PNCT (orange) and GzmB (green). The playback frame rate is 7 frames/s.

Video 5. **3D reconstruction of a representative CTL-APC conjugate formed with SAg-pulsed APCs.** CTLs were pre-treated with vehicle and used to form conjugates with SAg-pulsed Raji cells. Conjugates were co-stained for PNCT (orange) and GzmB (green). The playback frame rate is 7 frames/s.

Video 6. **3D reconstruction of a representative CTL-APC conjugate formed with SAg-pulsed APCs.** CTLs were pre-treated with Spike W and used to form conjugates with SAg-pulsed Raji cells. Conjugates were co-stained for PNCT (orange) and GzmB (green). The playback frame rate is 7 frames/s.